José Pedro Malanho da Silva

Degree in Biochemistry

Expression and purification of proteins involved in the mitochondrial electron transport chain
Biophysical characterization of a novel membrane mimicking system

Dissertation to obtain the Master degree in Biochemistry for Health

Supervisor: Dra. Manuela M. Pereira
Co-Supervisor: Dr. Afonso Duarte

Jury:

President: Doutor Pedro Matias
Opponent: Doutor Pedro Lamosa
Members of the jury: Doutora Margarida Archer

Instituto de Tecnologia Química e Biológica, António Xavier

December 2015

Expression and purification of proteins involved in the mitochondrial electron transport chain; Biophysical characterization of a novel membrane mimicking system

Agradecimentos

Agradeço a todas as pessoas envolvidas na realização do trabalho experimental e da escrita desta tese.

Agradeço em particular aos meus orientadores Dra. Manuela Pereira e Dr. Afonso Duarte por me terem acolhido no laboratório, pelas trocas de ideias, motivação e apoio durante a elaboração desta tese.

Agradeço também ao apoio incondicional dos meus pais, mana, namorada e família na concretização desta tese. Desde já peço desculpa pela minha ausência à família e namorada.

Por último agradeço a todos os meus amigos e colegas do laboratório pelos bons momentos e por me ajudarem nas situações difíceis da minha vida.

Abstract

NADH: ubiquinone oxidoredutase is one of the most intricate enzymes. It is part of the respiratory chains and is present in several organisms. This enzyme couples the transfer of two electron, from NADH to ubiquinone, and translocate ions across the membrane establishing a transmembrane difference of electrochemical potential. In this work, we present the initial experimental steps to express and purify a subunit from this intricate enzyme, which is directly related with the translocation of ions (i.e. NuoL). The objective was to characterize the subunit reconstituted in membrane-mimicking nanoparticles called nanodiscs using solution Nuclear Magnetic Resonance spectroscopy.

Nanodiscs are discoidal nanoparticles composed of lipids delimited by an amphipathic helical protein that stabilizes the lipidic hydrophobic chains.

In this work, we characterize nanodiscs composed by two types of lipids: POPC and *E. coli* lipids. The obtained Nanodiscs were studied at different temperatures using several techniques to determine the stability of Nanodiscs at high temperatures.

It was observed that with the increase of temperature, the amphipathic protein lose its secondary structure while the Nanodiscs increases in diameter. However, cooling the Nanodiscs to room temperature restores the membrane environment, as shown by ^{31}P-NMR spectroscopy. In this work, we show that the Nanodiscs are a suitable membrane platform, which can be used to characterize reconstituted protein in a wide range of temperatures.

Key words: NADH: ubiquinone oxidoredutase; Nanodiscs; circular dichroism; dynamic light scattering; thermal stability; lipids.

Resumo

NADH: ubiquinona oxidorredutase é umas das enzimas mais complexas da cadeia respiratória e está presente em vários organismos. Esta enzima acopla a transferência de dois eletrões, do NADH para a ubiquinona, e transloca protões através da membrana estabelecendo uma diferença de potencial eletroquímico transmembranar. Neste trabalho, são apresentados os passos experimentais iniciais para expressar e purificar uma subunidade desta enzima, que está diretamente relacionada com a translocação de iões (i.e. NuoL). O objetivo seria caraterizar a subunidade reconstituída num ambiente que mimetiza as membranas, i.e. nanodiscos, utilizando a espectroscopia de Ressonância Magnética Nuclear em solução.

Os nanodiscos são nanopartículas discoides compostas por lípidos e delimitadas por hélices anfipáticas que estabilizam as cadeias hidrofóbicas dos lípidos.

Neste trabalho foram caracterizados nanodiscos compostos por dois tipos de lípidos: POPC e lípidos de *E. coli*. O nanodiscos obtidos foram estudados a diferentes temperaturas usando diversas técnicas para determinar a estabilidade dos nanodiscos a altas temperaturas.

Foi observado que com o aumento de temperatura que a proteína anfipática perde a sua estrutura secundária, enquanto os Nanodiscos aumentam de tamanho. No entanto, após o arrefecimento para a temperatura ambiente os Nanodiscos recuperam o seu ambiente membranar, como é mostrado por espectroscopia de ^{31}P-RMN. Neste trabalho mostramos que os Nanodiscos são uma plataforma membrana capaz de ser usada para caracterizar proteínas reconstituídas numa ampla gama de temperaturas.

Palavras-chave: NADH: ubiquinona oxedorredutase; Nanodiscos; Espetroscopia de Ressonância Magnética Nuclear em solução; estabilidade térmica; lípidos

Contents

I. Figure Index

II.Table Index

III. List of abbreviations

ATP - Adenosine triphosphate

CA - Cardiolipin

CD – Circular Dichroism

CV - Column Volume

DLS – Dynamic Light Scattering

DMPC - 1,2-dimyristoyl-sn-glycero-3-phosphocholine

DPPC - dipalmitoylphosphatidylcholine

Fe-S - Iron-sulfur centers

FID - Free Induction Decay

FMN - Flavin mononucleotide

GFP – Green Fluorescence Protein

HL – Long Helix

HSQC - Heteronuclear Single Quantum Coherence Spectroscopy

HTP - Hydroxyapatite

IMAC - Immobilized Metal Affinity Chromatography

MSP – Membrane scaffold protein

MRP - Multiple resistance to pH

NMR – Nuclear Magnetic Resonance

NAD - Nicotinamide adenine dinucleotide

ND – Nanodisc

ND_E – *E. coli* lipid nanodiscs

ND_P – POPC lipid nanodiscs

Nqo - NADH quinone oxidoreductase

Nuo - NADH ubiquinone oxidoreductase

PE - L-α-phosphatidylethanolamine

PG - L-α-phosphatidylglycerol

POPC - 1-palmitoyl-2-oleoyl-sn-glycero-3-phosphocholine

Q - Quinone

QH2 - Quinol

RF - Radiofrequency

SAXS – Small Angle X-ray Scattering

TBS - Tris buffered saline

TM - Transmembrane

1 Aims and motivations

In the framework of the course "Biochemistry for Health", this thesis aimed at investigating ion translocation by respiratory Complex I. This complex couples the NADH:quinone oxidoreduction to ion translocation, contributing in this way to the establishment of a transmembrane difference on the electrochemical potential. Its mechanism of action is not understood. Complex I is present in the respiratory chain, from the mitochondria, and is related to several diseases such as Parkinson, Alzheimer and cancer. Bacterial Complex I is a suitable model for the study of mitochondrial Complex I since it is simpler and constituted by subunits composing the minimal functional "core" of eukaryotic Complex I. Specifically, one of the objectives of this work was the identification of the ion transport pathways in membrane subunits of Complex I. We also aimed to study these subunits in a membrane environment suitable to solution NMR characterization. For this, Nanodiscs were the membrane-mimicking environment elected whose characterization constituted another goal of the project.

1.1 Introduction

Bioenergetics is a field of biochemistry and biology that explores the processes related to energy conversion[1] and the intervening molecules, such as enzymes. Without energy, there is no life and nature developed enzymes capable of converting energy from different sources such as the sun or chemical compounds. The enzymes present in the respiratory chain are responsible for the conversion of energy from substrates to an electrochemical potential across the membrane.

The respiratory chain is present in the membrane of mitochondria, in eukaryotic organisms, and in the cytoplasmatic membrane, in prokaryotes. Figure 1.1 shows a schematic representation of the aerobic respiratory chain from *Escherichia coli*. This respiratory chain includes the membrane complexes: NADH: ubiquinone oxidoreductase; Succinate: quinone oxidoreductase and Ubiquinol oxidoreductase. This respiratory chain is fed with electrons from nicotinamide adenine dinucleotide (NADH) and succinate to NADH: ubiquinone oxidoreductase and to Succinate: quinone oxidoreductase, respectively. These two enzymes transfer the electrons from the respective substrates to ubiquinone reducing it to ubiquinol. Then ubiquinol diffuses through the membrane to Ubiquinol oxidoreductase, which oxidizes ubiquinol back to ubiquinone and reduces oxygen to water. The difference in reduction potentials between NADH and ubiquinone and ubiquinol and oxygen is high enough to allow the establishment of a transmembrane electrochemical potential, by translocating charges across the membrane.

The generated transmembrane difference of electrochemical potential is involved in several cellular processes, such as ion transport, substrate transport[2] and motility. In addition, ATPase can convert this membrane potential into chemical energy, in the form of adenosine triphosphate (ATP). ATP is an energetic molecule involved in cellular processes such as DNA and protein synthesis, signal transduction, and energy storage.

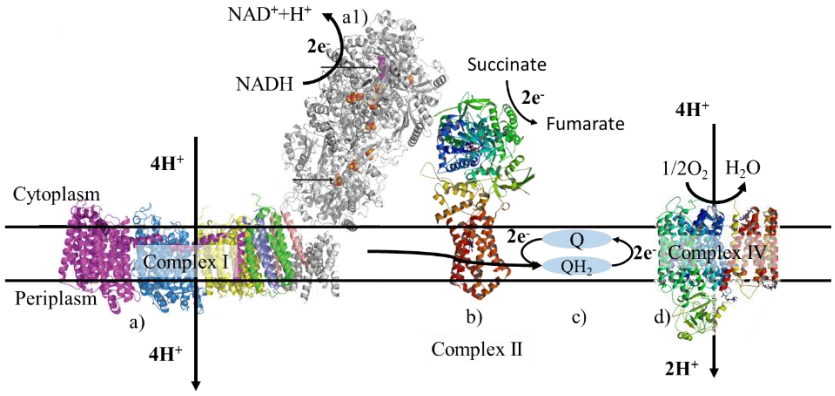

Figure 1.1: Schematic representation of the electron transport chain from *E. coli* with the known structures (adapted from[1]). a) NADH: ubiquinone oxidoreductase (membrane domain from *E. coli* and hydrophilic domain from *Thermus Thermophilus* [3]); b) succinate: quinone oxidoreductase (PDBID:2WDV); c) Q (Quinone) and QH2 (Quinol); d) Ubiquinol oxidoreductase (PDBID: 1FFT).

1.2 NADH: quinone oxidoreductase

NADH: quinone oxidoreductase, from the respiratory chain, is a membrane protein that is present in both prokaryotes and eukaryotes. For eukaryotes, this enzyme is called Complex I, it is present in the mitochondria, and is more intricate than the prokaryotes due to the extra subunits.

Complex I has an L-shape and is composed by two domains: one hydrophilic and one hydrophobic. The bacterial Complex I has a total of 550kDa and the mammalian has 980kDa. The hydrophilic domain is responsible for electron transfer and the membrane domain is responsible for the ion translocation[3–5]. The mechanism that allows the energy transfer, from the redox reaction, from the hydrophilic domain to the hydrophobic domain in order to establish a transmembrane difference of electrochemical potential, it is not clear.

NADH: ubiquinone oxidoreductase in *E. coli* (E.C.1.6.5.3) is composed of 13 subunits (two fused) where seven are hydrophilic and the other six are hydrophobic. These subunits, which are conserved in mitochondrial Complex I[6,7],constitute the called "core" subunits from a total of 44-45 [3,8], of eukaryotic Complex I. The remaining subunits are called supernumerary and the function of these subunits can be regulatory, stability and assisting in the assembly of Complex I[9]. Since the "core" subunits are considered the minimal functional unit then the catalytic and translocation mechanisms are similar in the prokaryotic and eukaryotic enzymes.

Table 1-1 shows the subunits from *E. coli* and the corresponding "core" subunits in the mitochondrial Complex I, from Bovine.

Table 1-1: Comparison of Complex I core subunits from *E. coli* and *Bos Taurus* (adapted from [10])

	E. coli	**Bovine**	**Prosthetic group**
Size	550kDa	980kDa	
Number of subunits	13	45	
	Hydrophilic domain		
Subunits	NuoF	51kDa	FMN, N3
	NuoE	24kDa	N1a
	NuoG	75kDa	N1b, N4, N5 and some species N7
	NuoDC	49kDa	
	NuoDC	30kDa	
	NuoB	PSST	N2
	NuoI	TYKY	N6a, N6b
	Hydrophobic Domain		
	NuoA	ND3	
	NuoH	ND1	
	NuoJ	ND6	
	NuoK	ND4L	
	NuoL	ND5	
	NuoM	ND4	
	NuoN	ND2	

The resolution of the crystallographic structure of Complex I was a major breakthrough to the field because it allowed the investigation of the catalytic and translocation mechanisms, including the putative ion channels. The published crystallographic structures, until now, are from *E. coli* (membrane domain)[3], *Thermus Thermophilus*[6] (whole enzyme) and *Yarrowia lipolytica*[11] (whole enzyme). A structure of Complex I from Bovine[12], using cryo-electron microscopy, was also obtained.

In this work, we focus on the respiratory Complex I of *Escherichia coli* because the subunits of this enzyme are conserved in the mitochondrial Complex I [6,7], making the NADH: ubiquinone oxidoreductase, from *E. coli*, a suitable model to characterize the translocation mechanism. The reduction potentials of NADH and ubiquinone are $E^{\circ\prime} = -0.320$ V[13] and $E^{\circ\prime} = +0.120$ V[13,14], respectively. The redox reaction between NADH and ubiquinone is thermodynamically favorable, allowing the conversion of energy to a transmembrane electrochemical potential by translocating three[15–19] to four protons[15,16,20] across the membrane. As previously referred, the mechanism of energy conversion is not known. However, there is a hypothesis where the energy released, from the redox reaction with the quinone, generates conformational changes, which propagates through the membrane part of the enzyme opening and closing ion accesses, like a piston mechanism[6].

NADH: ubiquinone oxidoreductase has: 8-10 iron-sulfur centers [Fe-S] (Figure 1.2 in orange and red), where at least two iron-sulfur centers are binuclear [2Fe-2S]$^{(+2/+1)}$ and at least six iron-sulfur centers are tetranuclear [4Fe-4S]$^{(+2/+1)}$[21]. This enzyme also contains one flavin mononucleotide (FMN) (Figure 1.2 in purple), a NADH/NAD$^+$ binding site, near FMN in the soluble part, and a quinone binding site in the interface of membrane and soluble domains.

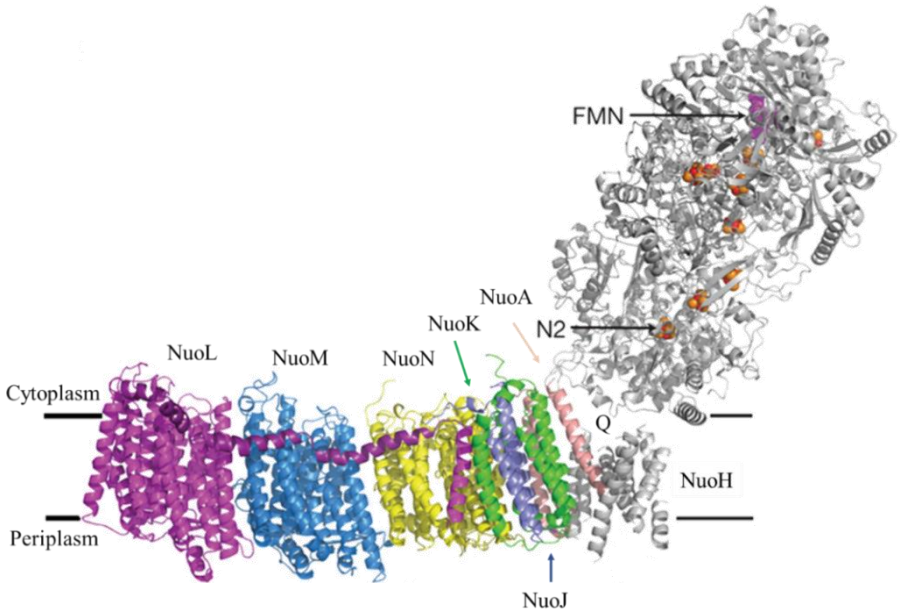

Figure 1.2: Cartoon representing bacterial Complex I. This structure was assembled with membrane domain from *E. coli* and hydrophilic domain from *Thermus Thermophilus*. In the hydrophilic domain is represented in purple the FMN and in orange and red the Fe-S clusters. Q represents the quinone binding site and N2 the last Fe-S that transfers the electrons to the quinone. (adapted from [3])

The subunits of NADH: ubiquinone oxidoreductase from *E. coli*'s are called Nuo and range from NuoA to NuoN[22]. The membrane domain is composed by the subunits L, M, N, A, J, K and H, making a total of 222kDa[3], with 55 transmembrane helixes. Sequence and structural analyzes show that three subunits NuoL, M and N are homologous to each[3]. It also shows that they are homologous to subunits of multiple resistance to pH (Mrp) which are Na^+/H^+ antiporters[6,23] suggesting that Complex I also may act as a Na^+/H^+ antiporter. In fact, a study that uses ^{23}Na NMR spectroscopy proves that Complex I is an antiporter and translocates sodium.[22]

1.2.1 NADH: ubiquinone oxidoreductase - NuoL Subunit

NuoL subunit is a membrane protein that has composed of sixteen transmembrane (TM) helixes and a long amphipathic helix, with interruptions, also known as long α-helix (HL) (Figure 1.3).

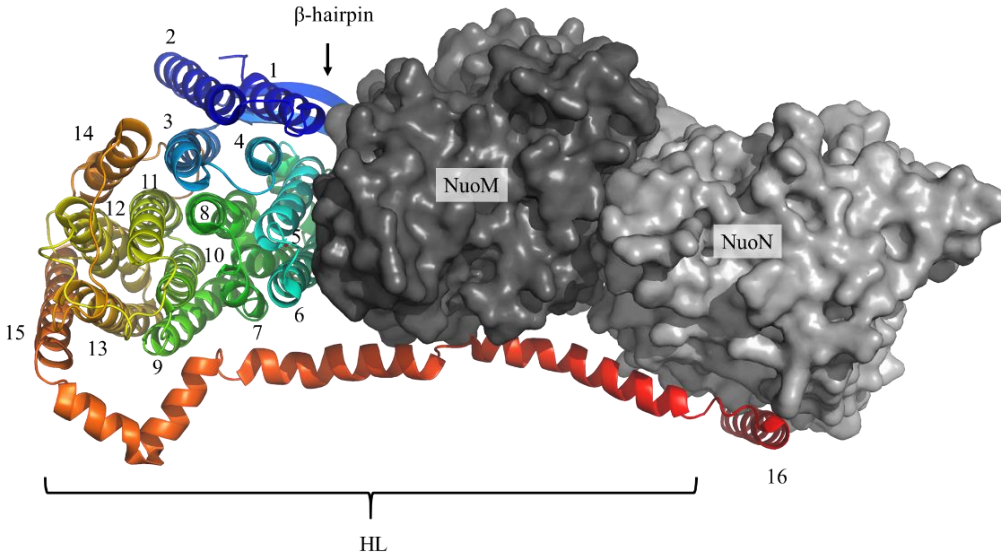

Figure 1.3: NuoL subunit from NADH: ubiquinone oxidoreductase (PDBID 3RKO chain L), from the cytoplasmatic view, with numbered helixes, β-hairpin and HL. In dark grey it is represented the surface of NuoM (PDBID 3RKO chain M) and in light gray it is represented the surface of NuoN (PDBID 3RKO chain N).

TM1, 2 and 14 are in the opposite side of HL and are the least conserved TMs (Figure 1.3) (The degree of conservation was calculated with an alignment of 30 sequences of Complex I subunits from representative organisms from all kingdoms of life)[24]. The polipeptidic chain between TM2-3 forms a β-hairpin at the periplasm surface and contributes to intersubunit interactions[10]. TMs 4-13 are the most conserved and form the core of subunit NuoL[3]. TM4-8 and TM9-13 have an internal symmetry and can be superimposed by performing a 180° rotation, along the membrane plane[3]. This kind of pattern in sequence and structure is what can be called structural repeats. With this and with the physical arrangement of TM4-8 and TM9-13 these are called inverted repeats.

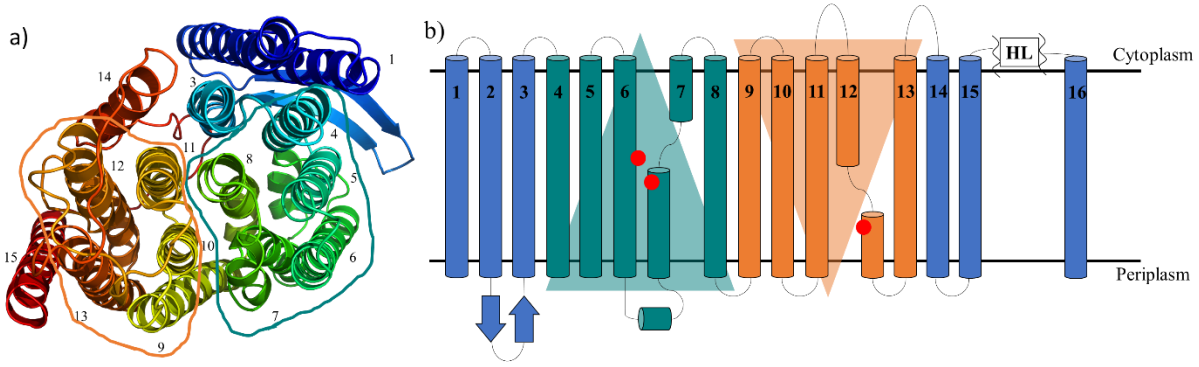

Figure 1.4: a) Representation of TM1-15 of NuoL of Complex I, from cytoplasmatic side. Inside the circles in color green (TM4-8) and in red (TM9-13) are represented the inverted repeats, b) topology diagram NuoL showing the different repeats (triangles and helices in green and orange), kinks in TM7 and TM12 and conserved residues (TM5 (E144), TM7 (K299) and TM12 (K399)) and in blue are the least conserved TMs.

In Figure 1.4 b) it is represented a topology diagram identifying the inverted repeats colored in green and orange. It is worth notice that TM7 and TM12 have a discontinuity called helical kinks, caused by

conserved proline residues, one in each TM helix. A kink and a polar residue in the middle of the membrane are energetically unfavorable meaning this structural feature is relevant in ion translocation. This structural characteristic is also present in other transporters. This type of discontinuity gives flexibility which is necessary for transport[25].

The translocation pathway of the ions, in NADH: ubiquinone oxidoreductase, is still under debate. This is due to the lack of a clear pathway in the crystallographic structures. However, some residues involved in the ion transport were identified by mutations and activity assays[26–28]. Efremov and Sazanov[3] propose a putative pathway (Figure 1.5) composed by two highly conserved half-channel. However, the crystallographic structure and by bioinformatics studies whose programs search cavities in proteins, show that these channels are not connected neither to the cytoplasm or periplasm[24].

These half channels are composed of polar and charged residues[3] (Figure 1.5 region I and II in green). The first half-channel comprising the residues H100; T120; S150 and K299 has a cavity with 70Å^3. In this cavity, there is a conserved lysine residue present TM7 (K299) and a glutamate residue in TM5 (E144), which electrostatically interacts with each other. This half-channel connects with the cytoplasm[3]. Mutations in those two residues led to a loss of dNADH oxidase activity and proton translocation [27,28], and also decreases the amount of assembled complex[27]. In Figure 1.5, it is also schematized an alternative channel in black (R115; E144; Y151; R155; T174; D178 and Y199), which is between subunits L and M[24]. The second half-channel is composed by polar and charged residues (T257; S311; Q315; T318; H334; H338; K342; K399; D400; T425; Y428; T429; E494 and S497) and has a cavity with 20nm. In this cavity, there is a conserved lysine in TM12 (K399), which is in a position symmetrically similar to K299. This half channel connects with the periplasm[3]. Mutations in K399 also lead to a decrease of assembled complex and dNADH oxidase activity[27]. The connection between these two half channels is established through polar and charged residues (H254; A255 and T312), with the exception of A255, which is apolar[3].

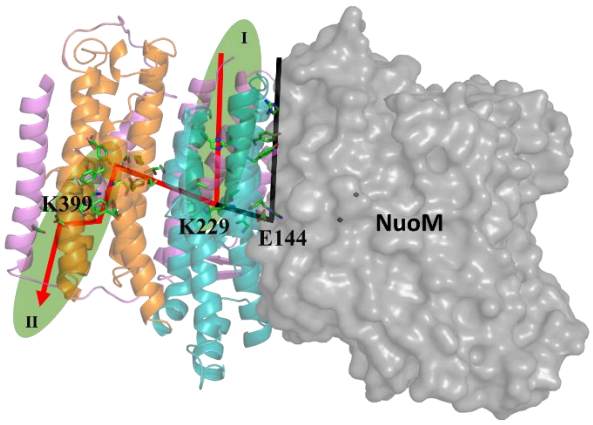

Figure 1.5: NuoL subunit (PDBID 3RKO chain L) and NuoM in grey. In NuoL there are represented the putative channels with highlight, in red and black, and conserved residues present in the cavities. The inverted repeats are represented in orange and teal. In green, the oval circles represent the first (I) and second (II) half channels with the conserved residues.

Another structural element of NuoL subunit is the long amphipathic helix HL that is 110 Å long. HL has polar residues that interact with the cytoplasm and apolar residues which interact with the membrane and with the subunits NuoM and N (via backbone and side chains)[3]. This is an indication that helix HL rests at the surface membrane. This amphipathic helix starts at the end of TM15, from NuoL, and ends at the beginning of TM16, which is anchored to NuoN, J and K. HL stabilizes the complex and interacts with conserved residues (Lys173, Asp246 and Tyr317) and a semi-conserved (His241) (66% conservation) of NuoM (conservation is in relation with these three subunits)[3]. Since this structural element connects with NuoM and NuoN it was suggested that helix HL could be a coupling element between the released energy from the redox reaction and the translocation of ions across the membrane[9].

1.2.2 Diseases in humans

In humans, several diseases have been associated with Complex I.

Complex I related diseases can have different origins caused either by mutations[29–31] or by the disassembly of Complex I[30]. Mutations can occur in the mitochondrial DNA or in the nuclear DNA, in supernumerary or core subunits[29] and in conserved or non-conserved residues[8]. In addition, these mutations can lead to a deficiency of Complex I where its activity is impaired[29–31]. Other mutations are not present in genes coding for Complex I but in genes coding assembly factors, which lead to an improper assembly[32].

Diseases related to Complex I are: Leber's hereditary optic neuropathy (LHON); Leigh syndrome; leukodystrophy; Parkinson's disease; Alzheimer's disease; Mitochondrial encephalomyopathy, lactic acidosis, and stroke-like episodes (MELAS); cardiomyopathy and even cause development delay[29,31,33]. Complex I[31,34] and Complex III[31] are responsible for the production of reactive oxygen species (ROS). These reactive species can damage lipids, proteins, DNA, leading to diseases, such as lactic acidosis and cardiomyopathy[31].

1.2.3 Nanodiscs

NuoL is a membrane protein and it requires a lipidic environment in order to be characterized. The study of membrane proteins is complex because they are difficult to express, purify and characterize. Main constrains are the extraction from the membranes and reconstitution in a stable membrane-mimicking environment. There are several examples of membrane mimicking environment and each one has advantages and disadvantages (Table 1-2). Some examples of membrane like environments are: detergent micelles[35 36], bicelles[37 38], vesicles[39], inverted micelles[40], organic solvents[41], amphipols[42], and nanodiscs[43–45].

Table 1-2: Advantages and disadvantages of different membrane mimicking environments.

Environment	Advantages	Disadvantages	References
Detergents	High solubilization ability. Some detergents are mild.	Denatures and deactivates protein.	46,47
Bicelles	Small particles for solution NMR. Controllable composition.	Only stable over a small range of temperatures	46
Inverted micelles	High solubilization High substrate concentration	Denaturing effect of surfactant Presence of organic solvent	40
Vesicles	Easy to use. Controllable composition. Lipidic inside and outside environment.	High molecular mass is not suitable for solution NMR. Protein orientation difficult to control.	48
Organic solvents	Some solvents are inexpensive	May denature proteins. Only suitable for small transmembrane proteins. May induce a non-native structure.	49
Amphipols	Stabilizes subunits of proteins.	Heterogeneous environment.	46
Nanodiscs	Monodisperse and flat lipid bilayer. Size, thickness and lipid composition are tunable.	Lack of lipidic inside and outside environment	50

We address protein reconstitution in the membrane by using the Nanodisc technology, because it allows a characterization of the reconstituted protein in a free detergent environment using solution Nuclear Magnetic Resonance spectroscopy. Nanodiscs are easy to implement, easy to manipulate and provide a native like environment, without detergents. This lipidic nanoparticle allows a biophysical characterization of the reconstituted protein by several methodologies such as circular dichroism and fluorescence spectroscopy besides Nuclear Magnetic Resonance spectroscopy[51,52]. Furthermore, the size of Nanodiscs, lipid and number of lipid composition is controllable. Table 1-2 shows that the Nanodiscs have a disadvantage, however it depends on type of the planned experiment. For this work, there is not a need for a compartmentalization, because the objective is to identify the transport pathway.

Nanodiscs (ND) are discoidal nanoparticles composed of an assembled bilayer of phospholipids and by amphipathic helical proteins termed membrane scaffold proteins (MSP)[43] (Figure 1.6) . Nanodiscs are formed by a process of self-assembly, which relies on the correct stoichiometry between phospholipids and MSP[50] to ensure a monodisperse solution of Nanodiscs with the expected size[43].

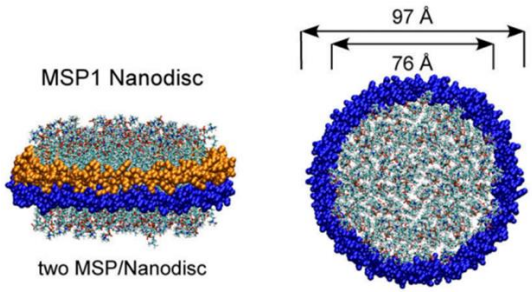

Figure 1.6: Representation of NDs from different perspectives: from the side (left) and from above (right). In blue and yellow are represented the two MSP and in the interior are the lipids (Image adapted from [53]).

MSPs are engineered proteins containing approximately 200 amino acid residues from the C-terminal of the human apolipoprotein A1, which is present in high-density lipoproteins. MSPs are composed of several amphipathic helixes, which interact with the lipids' aliphatic chain and with the buffer. The number of amphipathic helixes determines the different ND sizes. A longer MSP originates a larger ND. Similarly, the size of the NDs decreases if the MSP is shorter. The section of the MSP that is truncated is fundamental for this changing, for example the first 20 amino acids in N-Terminal have no role in the self-assembly of NDs, so if we remove them, it does not affect the size of the ND[44]. The MSP1E refers to an extension (E) of the MSP1 by inserting a repeat of a helix and MSP1D it is a deletion (D) in the MSP1[44].

There are several examples of different lipids used to produce a variety of NDs. For example dipalmitoylphosphatidylcholine (DPPC), 1-palmitoyl-2-oleoyl-sn-glycero-3-phosphocholine (POPC)[44] and 1,2-dimyristoyl-sn-glycero-3-phosphocholine (DMPC) (Figure 1.7) can be found in literature.

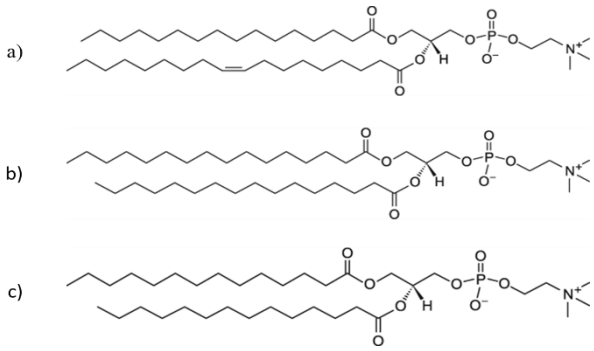

Figure 1.7: Structure representation of the most used lipids in NDs. a) 1-palmitoyl-2-oleoyl-sn-glycero-3-phosphocholine (POPC); b) dipalmitoylphosphatidylcholine (DPPC) and c) 1,2-dimyristoyl-sn-glycero-3-phosphocholine (DMPC).

The process of self-assembly of the NDs requires lipids and MSP in solution, in a defined stoichiometry. The process is initialized by detergent removal, using dialysis or porous polystyrene beads.

The lipids determine the thickness and the MSP determines the size of NDs. Table 1-3 shows the different sizes of NDs composed of different MSP, measured by small angle X-ray scattering (SAXS) and by the retention time in a size exclusion chromatography (Stokes' diameter). The Stokes' diameter is obtained by analyzing the elution profile of a sample and comparing the elution volume with those of standard proteins with a known Stokes' diameter.

Table 1-4 shows the lipid MSP stoichiometry for different MSPs and the incubation temperature for each lipid for the process of self-assembly. The incubation temperature is near the transition temperature of the lipids and this leads to an efficient Nanodiscs assembly. However, the reasons for this phenomenon are still unclear and it is hypothesized to be related to the size and organization of detergent micelles. [53]. In addition, above the transition temperature the membrane is more fluid and similar to a cell membrane.[54]

Table 1-3: Size of Nanodiscs composed by different MSP, independent from lipid composition. (* Literature did not allow an estimation of the standard deviation)

	MSP1	MSP1E1	MSP1E2	MSP1E3	References
Stokes' diameter (nm)	9.38±0.56	10.3±0.31	11.03±0.36	12.07±0.08	44,55
SAXS (radius) (nm)	4.3±0.50	4.60±0.40	5.15±0.35	5.45±0.53	44,55,56
SAXS (diameter) (nm)	9.75±0.05	10.6*	11.9*	12.9*	44

Table 1-4: Lipid to MSP stoichiometry of different lipids and MSP (mol/mol), per each leaflet.

	MSP1	MSP1E1	MSP1E2	MSP1E3	Incubation temperature	References
POPC	62±9	79±7	103±7	126±17	4°C	44
DPPC	84±7	106±1.5	134±3.3	167.8±8.7	37°C	44
DMPC	77±2	102.5±10	122±3	147.5±2	25°C	44,56

The study of heterogeneous composition of lipids in nanodiscs[57] is also described, as for more complex Nanodiscs that are composed by *E. coli* lipids[58-59]. According to Avanti, these are: L-α-phosphatidylethanolamine (PE); L-α-phosphatidylglycerol (PG); cardiolipin (CA) and some unknown lipids (see Table 1-5 for Avanti's *E. coli* lipid composition and Figure 1.8 for molecular structure of Avanti's *E. coli* lipids).

Table 1-5: *E. coli* Total extract phospholipid profile from Avanti.

***E. coli* Total extract phospholipid profile**	
Component	wt/wt (%)
PE	54.5
PG	15.1
CA	9.8
Unknown	17.6
Total	100

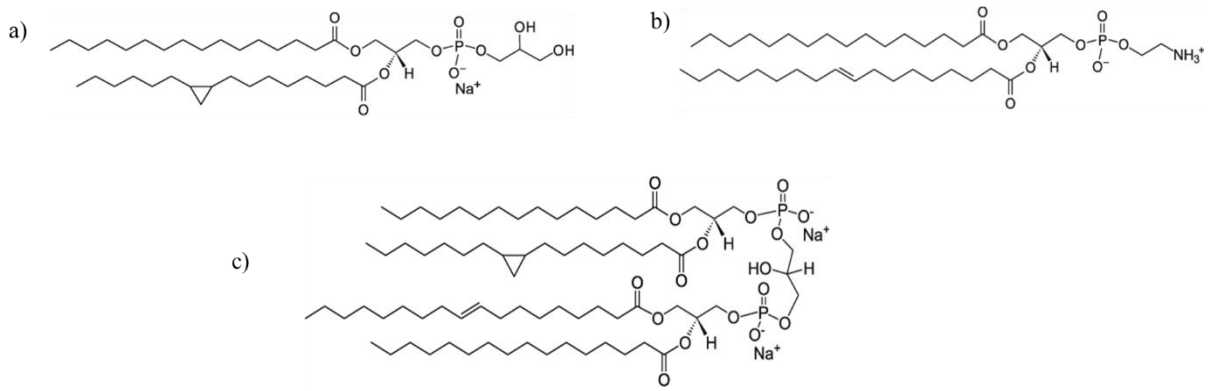

Figure 1.8: Structure of lipids *E. coli* Total extract (Avanti). a) Table of *E. coli* membrane lipid percentages, b) PE (L-α-phosphatidylethanolamine), c) PG (L-α-phosphatidylglycerol), d) cardiolipin

Some examples of the characterization of membrane proteins in Nanodiscs found in literature are: cytochromes P450[60], blood coagulation and human tissue factors[61], bacteriorhodopsin[52,55], receptors, (e.g. G-protein coupled receptor[62] and bacterial chemoreceptor[63]) and peptide translocon complex[64].
Nanodiscs are widely used in structural biology for the characterization of the reconstituted protein. Other applications than structural biology are: drug delivery[65] and screening[66], imaging[67] and electrical production[68].

2 Material and Methods

2.1 NuoL antiporter like subunit: expression and purification

2.1.1 Competent cells

E. coli C43 (DE3) (Lucigen Inc. USA) cells were inoculated in Lucia Broth (LB) medium and incubated overnight (37 °C, 150 rpm). One percent of the overnight growth was inoculated in Super Optimal Broth (SOB)[69] medium, supplemented with Mg^{2+}, and incubated at 37 °C, 150 rpm. When growth reached a cell density corresponding to OD_{600nm} of 0.6, the cell culture growth was stopped by placing it on ice for at least 10 min. Cells were harvested by centrifugation (2100 g, 10 min, 4 °C). Supernatant was discarded and cells were resuspended in 8 mL buffer (10 mM HEPES, 15 mM $CaCl_2$, 250 mM KCl, 55 mM $MnCl_2$ pH 6.7), incubated for 10 min on ice and centrifuged at 2100 g, 10 min, 4 °C. Supernatant was discarded and cells were resuspended in 2 mL buffer (10 mM HEPES, 15 mM $CaCl_2$, 250 mM KCl, 55 mM $MnCl_2$ pH 6.7). DMSO (from a 100 % stock) was added to the cells to a final concentration of 7 % and these cells were incubated on ice for 10 min. Cell aliquots of 100 µL were flash frozen with liquid nitrogen and stored at -80 °C.

2.1.2 Transformation and expression of NuoL constructs

The expression of the recombinant protein was achieved using *E. coli* C43 (DE3) cells in combination with the plasmid pJ421. The plasmid with the gene of interest was previously selected in the Biological Energy Transduction group and manufactured by DNA 2.0 Inc. USA. The gene of interest codes the NuoL subunit and two tags, the GFP and six-histidine residues that are located at the C-terminal and N-terminal respectively. Competent cells were transformed with the plasmid pJ421 using a heat shock protocol. Competent cells were incubated with 5-10 ng of DNA (quantified by UV-Visible spectroscopy) on ice for 30 min, followed by a 42 °C heat shock for 30 seconds and further incubation on ice for 2 min. Cells were inoculated in pre-warmed Super Optimal Broth with catabolite repression (SOC)[69] solution and incubated for 1.5 h at 37 °C, 300 rpm. Cells were harvested by centrifugation (13000 rpm, 5 min) and then resuspended in 50 µL of SOC medium. Cells were inoculated in LB-agar plates, supplemented with kanamycin (50 µg/mL), and incubated overnight at 37 °C, for selection of transformed cells. One colony from the LB-agar plates was inoculated in 100 mL of LB medium, supplemented with kanamycin (50 µg/mL), and incubated overnight at 37 °C, 180 rpm. The final overnight culture was used to inoculate a 2 L LB medium, supplemented with kanamycin (50 µg/mL), with a starting cell density of OD_{600nm} of 0.02. This cell culture was incubated at 37 °C, 120 rpm and the cell growth was monitored by the OD_{600nm}. When cell density reached OD_{600nm} of 0.6, isopropyl β-D-1-thiogalactopyranoside (IPTG) (Apollo Scientific limited) was added in a final concentration of 0.7 mM to initiate the expression of the recombinant protein. The cell growth continued overnight under the previous conditions. Cells were harvested by centrifugation (8000 rpm for 15 min at 4 °C), resuspended

in a 50 mM Tris-HCl, 300mM NaCl, pH 8 buffer supplemented with protein inhibitors (Roche Inc., USA) and stored at -20 °C.

To assess protein expression during cell growth, culture aliquots were collected from the inoculation point to the end of the culture growth. Cell disruption was achieved via freezing and thawing and disrupted cells were analyzed by fluorescence spectroscopy to detect the presence of Green Fluorescent Protein (GFP) by exciting the sample at 410 nm and measuring the emission spectra from 450 nm to 600 nm. GFP presents an emission maximum at 515 nm.

2.1.3 Purification of NuoL antiporter domains

E. coli C43 (DE3) cells previously harvested and stored at -20 °C were disrupted using a French press (10000 psi) apparatus or an APV-1000 (8000 psi) equipment. Disrupted cells were centrifuged (12000 rpm, 10 min, 4 °C) and the supernatant was ultracentrifuged (42000 rpm, 2 h, 4 °C), to separate the soluble fraction from the membranes. The supernatant was discarded and membranes were resuspended, using a Potter-Elvehjem homogenizer, in 50 mM Tris-HCl, 2 M NaCl pH 8. High ionic strength allows removing of proteins that interact weakly with the membrane. The membrane fraction was ultracentrifuged (42000 rpm, 2 h, 4 °C), the supernatant was discarded and the membranes were washed with 50 mM Tris-HCl pH 8 buffer to decrease the ionic strength to 500 mM NaCl.

Total amount of membrane protein was assessed by the biuret method. Membranes were solubilized by gentle addition of n-Dodecyl β-D-Maltopyranoside (DDM) (GLYCON Biochemicals GmbH, Germany) in a 1:3 ratio (protein mass/ DDM mass) and incubated overnight at 4 °C with agitation. The membrane solution was ultracentrifuged (42000 rpm, 2 h, 4 °C) in order to separate solubilized from non-solubilized membranes. The pellet (non-solubilized membranes) was discarded and the solubilized membranes were stored at 4 °C for further studies.

2.1.3.1 Protein purification by affinity chromatography

Immobilized Metal Affinity Chromatography (IMAC) column with a total volume of 26 mL and connected to an AKTA Purifier (GE Healthcare) was used to purify the NuoL repeat. The column was activated with $NiSO_4$, followed by equilibration with buffer A (50 mM Tris-HCl, 500 mM NaCl, 0.05 % DDM pH 8).

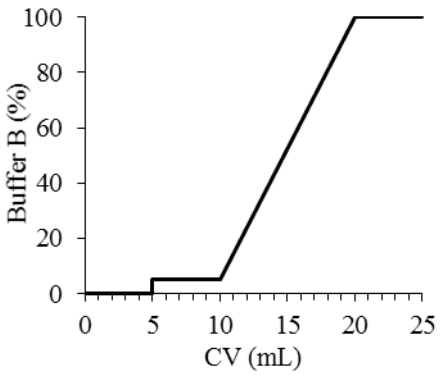

Figure 2.1: Schematic representation of IMAC chromatography elution gradient with buffer B (50 mM Tris-HCl, 500 mM NaCl, 500 mM Imidazole, 0.05 % DDM pH 8 at 4 °C).

The sample containing the solubilized membranes with NuoL repeat was injected in the column and it was eluted using a gradient of buffer B (buffer A with 500 mM imidazole) as described in Figure 2.1. Initially the column was washed with buffer A until absorbance at 280 nm stabilized, this allowed an initial removal of proteins that do not interact with the resin. A 5 % buffer B step was performed for 5 CV to elute proteins that interact weakly with the resin. The next step in elution was performed from 5 % to 100 % buffer B for 10 CV. Finally, the column was washed for 5 CV with 100 % of buffer B. During the elution, a flow rate of 3 mL/min and a maximum pressure of 0.4 MPa were used.

The collected fractions were analyzed by: a) Fluorescence spectroscopy (to assess GFP content using Varian Cary Eclipse Fluorescence Spectrophotometer); b) UV-Visible spectroscopy (to assess cytochrome contamination and GFP presence using Shimadzu UV-1700), c) SDS-PAGE (to assess number of contaminants) and d) Western Blot (WB) (to confirm the presence of GFP and/or His-tag). Fractions with same spectral UV-Visible profile were combined, concentrated and stored at 4 °C for further purification.

2.1.3.2 Protein purification by hydroxyapatite column

Hydroxyapatite (HTP) column with a total volume of 22 mL and connected to an AKTA Purifier 10 (GE Healthcare) was equilibrated with buffer C (20 mM potassium phosphate, 0.05 % DDM, pH 7.6) was used to purify the NuoL construct.

The fractions obtained in the IMAC chromatography were buffer exchanged to 20 mM potassium phosphate, 0.05 % DDM, pH 7.6, as the gradient in the HTP column was performed with phosphate buffer to 1 M of potassium phosphate. The elution gradient used in the HTP as described in Figure 2.2.

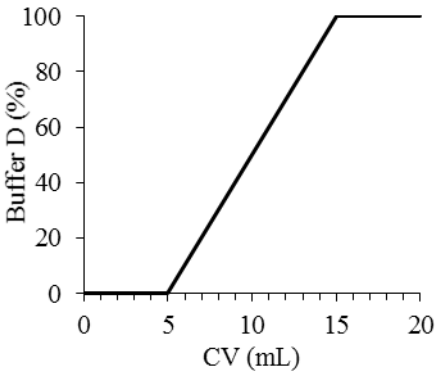

Figure 2.2: Schematic representation of HTP chromatography elution gradient with buffer D (1 M potassium phosphate, 0.05 % DDM pH 8 at 4 °C)

After sample injection, the column was washed with 5 CV of buffer C to elute the proteins that do not interact with the resin. Following this step, a phosphate gradient was performed for 10 CV from 0 % to 100 % with buffer D (1 M potassium phosphate, 0.05 % DDM,

pH 7.6). Finally, the column was washed with 5 CV of 100 % Buffer D. The elution steps were performed with a flow rate of 3 mL/min with a maximum pressure of 5 MPa. Collected fractions were analyzed by: a) Fluorescence spectroscopy, b) UV-Visible spectroscopy, c) SDS-PAGE and d) Western Blot.

2.1.3.3 Western Blot

An initial SDS-PAGE containing the samples under the study and the molecular mass markers (NZIColourProtein Marker II) was performed at 180 V, 400 mA and 100 W for 1 h. SDS-PAG was soaked in transfer buffer (100 mM Tris-HCl, 100 mM NaCl, 5 mM $MgCl_2$ pH 9.5) and placed in a Western Blot (WB) device (Transfer Blot SD Semi dry transfer blot (Bio-Rad)) with filter paper and with a nitrocellulose membrane. Proteins were transferred to the nitrocellulose membrane for 30 min at 15 V.

After protein transfer, the nitrocellulose membrane was soaked with 5 % (m/V) skim milk, in Tris Buffered Saline (TBS) (20 mM Tris-HCl, 100 mM NaCl, pH 7.6) for 30 min. Proteins in the nitrocellulose membrane were incubated with primary antibody against GFP (rabbit) with a dilution of 1:10000 in 5 % skim milk in TBS. The nitrocellulose membrane was washed three times with Tween20 in TBS for 10 min to remove the excess of primary antibody. The membrane was incubated with secondary antibody against rabbit (goat) with a dilution of 1:7500 in TBS and 5 % skim milk. In order to remove the excess of secondary antibody, a second washing procedure was performed. The detection of the GFP was achieved by adding a solution of BCPiP+NBT (Roche) to the nitrocellulose membrane, which was incubated for 15 min. The reaction was stopped with bidistilled water and by discarding the detection solution.

2.2 Nanodiscs: Assembly process

2.2.1 Expression of MSP1E1

For the expression of MSP1E1, *E. coli* (BL21-DE3 (GOLD)) cells stored at -80 °C and containing the plasmid pET 28a plasmid (supplied by Novagen) with the coding sequence of MSP1E1, were used. The cells stock was inoculated in 50 mL LB medium, supplemented with kanamycin (50 µg/mL), and incubated overnight at 37 °C, 180 rpm.

The overnight cell culture was used to inoculate a 800 mL LB medium, supplemented with kanamycin (50 µg/mL) with a starting cell density of OD_{600nm} 0.02. This new cell culture was incubated at 37 °C, 180 rpm and when the cell density reached $OD_{600\,nm}$ of 0.6-0.8, IPTG was added in a final concentration of 0.5 mM in order to initiate the expression of MSP1E1. The cell culture was incubated for 4 h at 37 °C, 180 rpm. After 4 h, the cell growth was stopped and the cells were harvested by centrifugation (8000 rpm for 15 min at 4°C). Cells were resuspended in 40 mM Tris-HCl, 300 mM NaCl pH 8, supplemented with protein inhibitors (Roche, GmbH, Germany), and stored at -20 °C.

When needed, cells were disrupted using either a French Press (10000 psi) apparatus or an APV-1000 (8000 psi) equipment. Intact cells were separated from centrifugation (8000 rpm, 10 min, 4 °C) and the supernatant, containing the lysed cells, was ultracentrifuged (42000 rpm, 2 h, 4 °C) in order to separate soluble fraction from membranes. Membranes were discarded and the supernatant was stored at 4 °C, for further procedures.

Expression of labelled ^{15}N-MSP1E1 followed the same protocol except that instead of LB medium M9 minimal[69] ($^{15}NH_4Cl$) medium was used.

2.2.2 Purification of MSP1E1 by affinity chromatography

IMAC column with a total volume of 26 mL and connected to an AKTA Purifier (GE Healthcare) was used to purify the MSP1E1. The column was activated with $NiSO_4$, followed by equilibration with buffer E (40 mM Tris-HCl, 300 mM NaCl pH 8).

Previously stored soluble fraction was injected in the equilibrated IMAC column and the protein was eluted using a gradient as schematized in Figure 2.3. Initially the column was washed with buffer E until absorbance at 280 nm stabilized, this allowed an initial wash of proteins that do not interact with the resin.

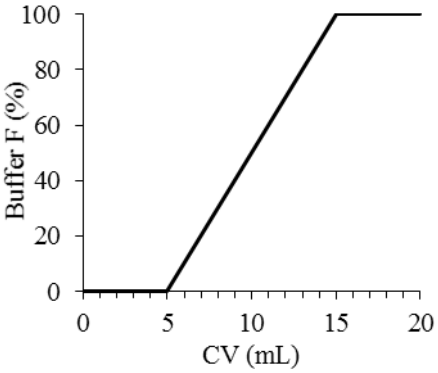

Figure 2.3: Schematic representation of IMAC chromatography elution gradient with buffer F (40 mM Tris-HCl, 300 mM NaCl, 500 mM Imidazole, pH 8 at 4 °C).

Then, a gradient for 10 CV from 0 % to 100 % of buffer F (buffer E with 500 mM imidazole) was performed. Finally, the column was washed for 5 CV with 100% of Buffer F. During the elution a flow rate of 3 mL/min and with a maximum pressure of 0.4 MPa were used.

Collected fractions were analyzed by SDS-PAGE. The fractions that presented the same SDS-PAGE profile were combined, concentrated and stored at 4 °C.

2.2.3 Nanodiscs setup

The POPC (Avanti Inc. USA) or *E. coli* lipid extract (Avanti Inc. USA) were dissolved in chloroform and stored at −20 °C in a glass vial. A lipid solution corresponding to 25 mg of lipids was dispensed to a round glass flask for chloroform evaporation in a rotary evaporator (Buchi) during 20 min. Reconstitution buffer (50 mM Tris-HCl, 300 mM NaCl, pH 8) with 250 mM sodium cholate was added to the lipids in a 1:2 proportion (lipid/sodium cholate (mol/mol)). Then the MSP was added to the mixture in the desired amount. For Nanodiscs with POPC the ratio MSP1E1:lipid was 1:80 (mol/mol) and for those containing *E. coli* lipids the ratio was 1:100 (mol/mol). The reconstitution mixture was diluted to a final concentration of cholate of 14 - 40 mM and it was incubated at a specific temperature depending on the used lipids (4 °C for POPC and 37 °C for *E. coli* lipids).

After incubation, hydrated Biobeads were added to the mixture (500-800 mg for each 1 mL of mixture volume) for detergent removal, in order to initiate the process of self-assembly. Then the solution was incubated for the desired amount of time at room temperature with shaking (4 h for POPC and 2 h for the remaining lipids). Afterwards, Biobeads were removed and washed with reconstitution buffer. Obtained Nanodiscs were stored at 4 °C for the next purification step.

2.2.4 Nanodiscs' purification protocol

A 24 mL Superdex 200 10/300 GL column connected to an AKTA Purifier 10 (GE Healthcare) was equilibrated with reconstitution buffer (50 mM Tris-HCl, 300 mM NaCl pH 8 at 4 °C). The previously prepared Nanodiscs were concentrated and injected in the column. An elution with reconstitution buffer was performed for 1.2 CV. The elution was performed with a flow rate of 0.5 mL/min with a maximum pressure of 1.5 MPa. Alternatively, a 290 mL Superdex 200 column was used, with a 0.5 mL/min with a maximum pressure of 0.5 MPa.

Collected fractions were analyzed by SDS-PAGE. Fractions were combined according to the SDS-PAGE profile and to the elution volume and concentrated to a final volume of 450 µL.

2.3 Biophysical characterization of Nanodiscs

2.3.1 Fluorescence spectroscopy

Fluorescence spectra were measured in a Varian Cary Eclipse Fluorescence Spectrophotometer equipped with a Peltier temperature controller. For all measurements, 5 nm slits were used and an excitation wavelength of 280 nm (to excite the tryptophans) and fluorescence emission was measured in the 300-450 nm range. Samples were prepared in 50 mM Tris-HCl, 300 mM NaCl pH 8 at 4 °C.

The purified Nanodiscs and MSP1E1 samples were diluted to a final concentration of 10 µM. Temperature dependent curve for MSP1E1 was performed from 10 to 80 °C with a 1 °C increment per minute and fluorescence intensity was measured at 340 nm. The temperature dependence curve for purified Nanodiscs was performed in the following procedure: Nanodisc sample was incubated at room temperature for 5 min and another 5 min at the desired temperature, prior to measurement. This procedure was performed to obtain emission spectra at temperatures ranging from 10 °C to 80 °C. Duplicate measurements of samples were obtained at each temperature.

2.3.2 Circular Dichroism

Circular Dichroism spectra were measured with a Jasco J-815 Circular Dichroism Spectropolarimeter equipped with a Peltier temperature controller. For all samples, the measured absorbance spectra ranged from 200-260 nm. Samples were prepared in 50 mM Tris-HCl, 300 mM NaCl pH 8 at 4 °C.

Purified MSP1E1 sample was diluted to 6.15 µM and absorbance spectra were acquired with 100 scans at a scan rate of 100 nm/min. A temperature dependent experiment was performed from 10 to 80 °C with 10 °C increments with 5 min of temperature equilibration prior to acquisition.

Purified Nanodiscs were diluted to 1 µM and incubated at room temperature for 5 min and another 5 min at the required temperature, prior to analysis. Absorbance spectra of independent Nanodiscs solutions were acquired with 50 scans at a rate of 50 nm/min and from 10 °C to 80 °C.

2.3.3 Dynamic Light Scattering

Dynamic light scattering was used to determine the size of Nanodiscs using a ZETASIZER Nano series (Malvern) equipped with a Peltier temperature controller. Samples were prepared in 50 mM Tris-HCl, 300 mM NaCl pH 8 at 4 °C. Purified Nanodiscs solutions were filtered with a 22 µm filter and diluted to 10 µM. Prior to measurement, the samples were incubated 5 min at room temperature and another 5 min at the required temperature.

Temperature dependence experiments were performed with independent samples, from 10 °C to 80 °C, 120 scans and 10 seconds/scan in a quartz cuvette. Quadruplicates measurements for each temperature were acquired.

2.3.4 UV-Visible spectroscopy

The UV-Visible absorbance spectra were measured using a Shimadzu spectrophotometer and the temperature was controlled using a Thermopar and Thermomixer. For all measurements, the absorbance was measured between 250-700 nm. Samples were prepared in 50 mM Tris-HCl, 300 mM NaCl pH 8 at 4 °C.

Purified Nanodiscs and free MSP1E1 samples were diluted to 10 µM, incubated for 5 min at room temperature and another 5 min at the required temperature prior to analysis. Independent samples were measured at temperatures ranging from 10 °C to 75 °C in a quartz cuvette with a 1 cm optical path length. Triplicates measurements for each temperature were acquired.

2.3.5 Stokes' radius and molecular mass determination

To determine the Stokes' radius and the molecular mass of Nanodiscs samples a Superdex 200 10/300 GL column with a total volume of 24 mL was used. The column was connected to an AKTA Purifier 10 (GE Healthcare) and equilibrated with Nanodiscs reconstitution buffer (50 mM Tris-HCl, 300 mM NaCl pH 8 at 4 °C). The previously purified Nanodiscs were concentrated, injected in the column and eluted for 1.2 CV with reconstitution buffer. The elution was performed with a flow rate of 0.5 mL/min with a maximum pressure of 1.5 MPa.

Two calibration curves were constructed to determine the molecular mass and the Stokes' radius of Nanodiscs. The calibration curves were calculated using: Apoferritin (440 kDa and 6.1 nm)[70]; Catalase (221 kDa and 5.22 nm)[71]; Glucose Oxidase (186 kDa and 5.2 nm)[70]; Aldolase (158 kDa and 4.81 nm)[71]; Conalbumin (77 kDa and 3.6 nm)[72] and Ovalbumin (44 kDa and 3.05 nm)[71]. The Stokes' radius and molecular mass of the Nanodiscs were assessed by combining the elution profiles and the Stokes' radius or molecular mass from protein standards. To determine the Stokes' an initial estimation of K_{AV} (partitions' constant) is made via eq. 1.1.

$$K_{AV}=(V_e-V_o)/(V_t-V_o) \quad \text{(eq. 1.1)}$$

Where V_e is the elution volume, V_0 is the void volume of the column and V_t is total volume of the column.

With K_{AV} a chart can be plotted, where $(-\log K_{AV})^{1/2}$ as function of Stokes radius for standard proteins.

2.3.6 NMR spectroscopy experiments

All NMR spectroscopy experiments were performed at the ITQB magnetic resonance center, CERMAX using standard Bruker pulse programs[73].

Purified MSP1E1, ^{15}N-MSP1E1, POPC Nanodiscs (ND_P) and *E. coli* lipid Nanodiscs (ND_E) samples were prepared in 10 % D_2O/ 90 % buffer. Buffer composition changed according to the experience and it was titrated to work at 4 °C. Two-dimensional ^{1}H-^{15}N and ^{1}H-^{13}C HSQC NMR spectra were collected at 25 °C on a Bruker Avance III 800 spectrometer (Bruker, Rheinstetten, Germany) with a TXI probe. ^{1}H-^{13}C HSQC spectra were collected for MSP1E1 sample (10 % D_2O/ 90 % 50 mM NaH_2PO_4, 300 mM NaCl pH 8) using "hsqcetgpsisp" pulse program with a delay (P1) of 9.58 µs. ^{1}H-^{15}N HSQC spectra were collected for ^{15}N-MSP1E1 sample (10 % D_2O/ 90 % 50 mM NaH_2PO_4, 300 mM NaCl pH 8) using a "hsqcetf3gpsi" pulse program with a delay (P1) of 9.53 µs. ^{1}H-^{13}C HSQC spectra were collected for ND_P sample (10 % D_2O/ 90 % 50 mM NaH_2PO_4, 200 mM NaCl, pH 7.5) using "hsqcetgpsisp" pulse program with a delay (P1) of 10.15 µs. ^{1}H-^{13}C HSQC spectra were collected for ND_E (10 % D_2O/ 90 % 40 mM NaH_2PO_4, 200 mM NaCl, pH 7.5) using "hsqcetgpsisp" pulse program with a delay (P1) of 9.63 µs. One dimensional ^{31}P NMR spectra were collected at different temperatures on a Bruker Avance III 500 spectrometer (Bruker, Rheinstetten, Germany) with a 31P SEX P-H-D probe using a "zgprde" pulse program with a delay of 8.00 µs. Samples were prepared in 10 % D_2O/ 90 % buffer 10 mM NaH_2PO_4, 40 mM Tris-HCl, 300 mM NaCl pH 8.

3 Results and discussion

3.1 NuoL expression and purification

One of the objectives of this thesis was to identify the amino acid residues involved in the ion translocation by NuoL subunit of Complex I from *E. coli*. To approach this objective several protein constructs were designed. In this thesis, we present the work developed with the construct spanning the TM9-13 region, which corresponds to the second repeat of NuoL. This construct also contains two tags: a GFP and six-histidine residues that are located at the C-terminal and N-terminal respectively. The six-histidine residue tag was introduced to improve the purification processes, while the GFP tag was included to facilitate the expression of the protein, to assist on the folding[74] of the protein and to allow monitoring the protein expression by fluorescence spectroscopy.

The expression of the second repeat construct was performed as described in the Material and Methods.

Table 3-1: Optical density measurements at 600 nm at different time points during a period of 24 h, after inoculation.

Time (h:min)	$OD_{600\ nm}$	Observations
1	0.08	-
2:45	0.4	-
3:15	0.77	Induction with 0.7 mM IPTG
23:45	3.52	-

The cell growth was monitored over time and Table 3-1 shows the optical density of transformed *E. coli* C43 (DE3) cells grown in LB medium at 37 °C for 24 h. At the end of the growth, the cell culture presented a cell density approximately of $OD_{600\ nm}$ of 3.5.

By SDS-PAGE no protein band with a higher intensity, possibly indicating the protein expression was detected. To confirm whether the construct was expressed, the fluorescence of the GFP was measured at different time points of the growth (before induction and at the end of the cell culture growth).

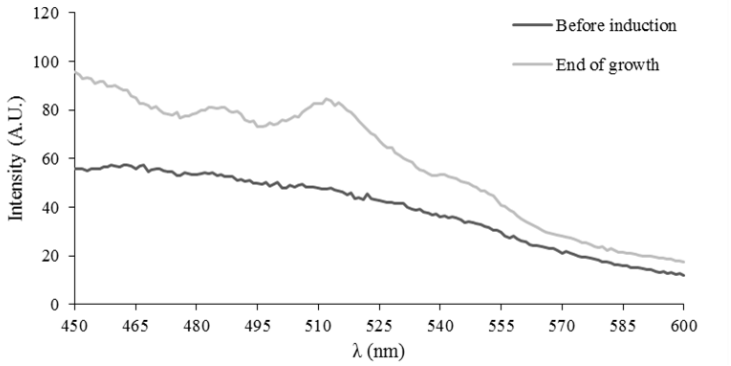

Figure 3.1: Fluorescence spectra of aliquots retrieved during cell culture growth. Samples were excited at 403 nm and fluorescence spectra were collected from 450 nm to 600 nm.

The fluorescence spectrum of the sample collected before the induction did not present a band with a maximum at 515 nm (see Figure 3.1 dark grey). This means that there was no basal expression of the construct, prior to protein expression induction. The fluorescence spectrum of the final point of the cell growth presented a band with a maximum at 515 nm, suggesting that GFP and consequently the rest of the construct were expressed (see Figure 3.1 light grey).

After confirmation of the expression of the NuoL construct, cells were disrupted and solubilized membranes were obtained as described in Material and Methods. The solubilized membranes were subjected to two chromatographic steps.

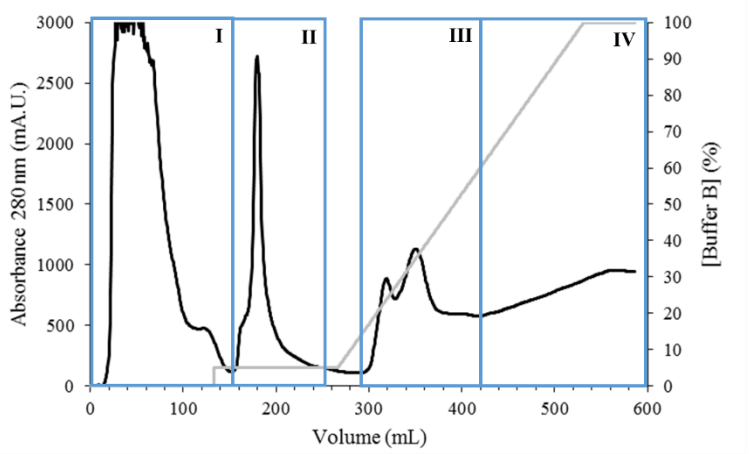

Figure 3.2: IMAC's (26 mL) chromatogram of solubilized membranes in 50 mM Tris-HCl, 500 mM NaCl, 0.05 % DDM, pH 8. The black trace represents the absorbance at 280 nm and the grey line the percentage of buffer B (50 mM Tris-HCl, 500 mM NaCl, 500 mM imidazole, 0.05 % DDM, pH 8). The boxes refer to the obtained fractions.

The first step was performed in an IMAC column. The chromatogram (Figure 3.2) shows the elution profile indicating that several proteins eluted at different percentages of buffer B. At 0 % buffer B, the proteins that did not interact with the resin were eluted. Increasing buffer B to 5 % lead to further elution of weakly interacting proteins. When a gradient from 5 % to 100 % of buffer B was performed, two bands, corresponding to proteins that strongly interact with resin were obtained. The construct strongly interacts with the resin due to the presence of his tag thus the elution of the construct is expected to take place in the imidazole gradient step. From 420 mL and forward, the absorbance linearly increases with the increase in concentration of imidazole. UV-Visible spectroscopy confirmed that imidazole absorbs at 280 nm and this could imply that from 420 mL and forward there was no elution of proteins.

To study the presence of the construct, fluorescence and UV-Visible spectroscopies were used to detect the presence of the GFP tag. Fluorescence spectroscopy showed that there is a band with a maximum at 515 nm in every fraction with UV-Visible absorbance at 280 nm. This suggests the construct's presence of in every fraction that has absorbance at 280 nm, i.e. in fraction I to IV.

In Figure 3.2, the blue boxes represent the selected fractions for analysis. The fractions were selected based on two criteria: percentage of imidazole and UV-visible spectra. The fractions were obtained as

follow: fraction I (0 % imidazole), fraction II (5% imidazole), fraction III and IV (UV- Visible spectra). For fraction III, the UV-Visible spectra revealed that cytochrome was present, as maximum characteristic peaks of these proteins were observed at 530 nm and 560 nm. This suggests that the cytochrome can strongly interact with the resin or it may interact with the construct. UV-Visible spectrum from fraction's IV measured absorbance at 280 nm and near 403 nm (which is characteristic of GFP).

To confirm the presence of the construct, a Western Blot (WB) analysis was made using a specific antibody that interacts with GFP.

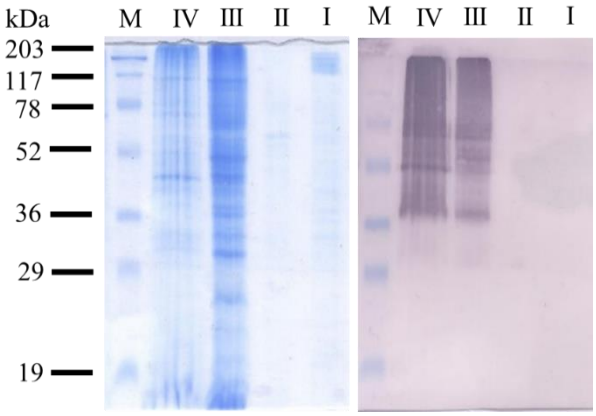

Figure 3.3: SDS-PAG (left) and WB (right) of the obtained IMAC's fractions (Figure 3.2). M – molecular mass marker; roman numerals correspond to the fraction of previous chromatogram (see Figure 3.2).

The SDS-PAG showed several bands in the different lanes, meaning that fractions not are pure. The WB (Figure 3.3) confirms the presence of GFP due to the existence of reactive bands present in fractions III and IV, suggesting that the construct fully interacts with the resin. WB of fractions III and IV presented a smeared pattern as if the wells were overloaded. To assess this hypothesis, the same sample was injected with different dilutions however, the results did not change. Several hypotheses can justify this observation: oligomerization of the second repeat, unknown interactions between the different proteins present in the fractions, or that the WB's conditions (e.g. antibodies' concentration) need optimization.

For the second step of purification, the fractions from IMAC were injected in HTP column.

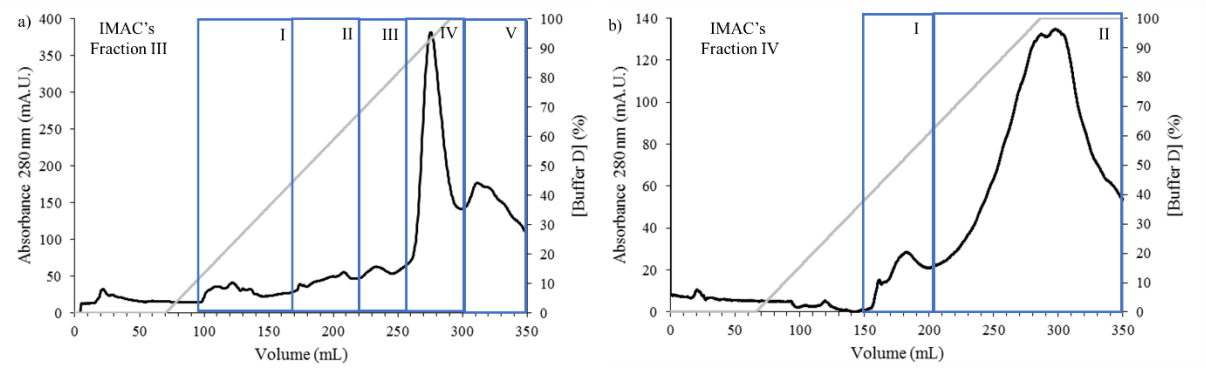

Figure 3.4: HTP chromatogram of fractions III (a) and IV (b) of IMAC's chromatogram. In black is represented the absorbance at 280 nm and in grey the percentage of buffer D (1 M potassium phosphate, 0.05 % DDM, pH 7.6). The boxes represent the fractions represent in which the chromatograms' fractions were divided.

Chromatograms from HTP column, of fractions III and IV from the IMAC, are represented in Figure 3.4 a) and b) respectively. Both chromatograms show different proteins elute at different percentages of buffer D. Fluorescence spectroscopy revealed the presence of a band with a maximum at 515 nm in all fractions. UV-Visible spectroscopy showed that fraction IV from Figure 3.4 a) had a characteristic UV-Visible spectrum of cytochrome Based on this information, the criteria for the separation of fractions was the elution volumes represent as blue boxes in Figure 3.4.

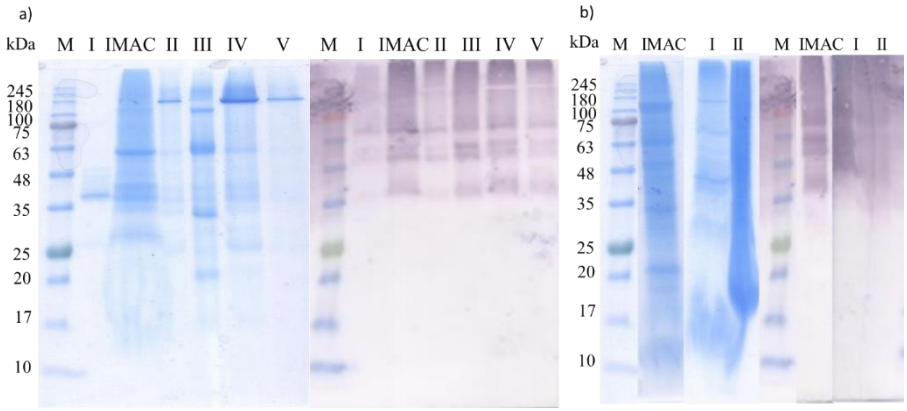

Figure 3.5: a) SDS-PAG (left) and WB (left). M- High molecular mass marker and roman numerals correspond to the fraction of previous chromatogram; b) SDS-PAG (left) and WB (left). M- High molecular mass marker and roman numerals correspond to the fraction of previous chromatogram.

In order to confirm where the construct eluted, SDS-PAGE and WB were performed (see Figure 3.5). SDS-PAG of the fractions from HTP chromatography presents several bands in each lane, demonstrating that the construct is not pure. WB shows that fractions from HTP have the same pattern as the fractions from IMAC, indicating that the construct is eluted in every fraction.

Due to the small amount of protein recovered in the last purification step, no further chromatographic methods were tested.

The purification of NuoL (TM9-13) construct was not successful. In order to overcome this situation, it is necessary to start with a larger quantity of target protein to optimize the purification processes. To achieve a larger expression of protein, further expression tests must be attempted. Some conditions

possible to optimized are: temperature of growth, temperature used after induction, concentration of IPTG, aeration of the cultures and time of expression after induction. Some of these conditions were tested, such as time after induction, e.g. 6 h and 10 h. However, no peak at 515 nm was observed by fluorescence spectroscopy of this expression test, meaning that in these conditions there is no expression of the construct.

3.2 Characterization of Nanodiscs

3.2.1 Expression and purification of MSP1E1

One objective of this thesis was to characterize the Nanodiscs membrane-mimicking environment. The Nanodiscs are constituted by lipids and held together by the membrane scaffold proteins (MSPs). In this work, the MSP used was the MSP1E1 and it was expressed using *E. coli* BL21-DE3 (GOLD) system. The expression of the protein was performed as described in the Materials and Methods.

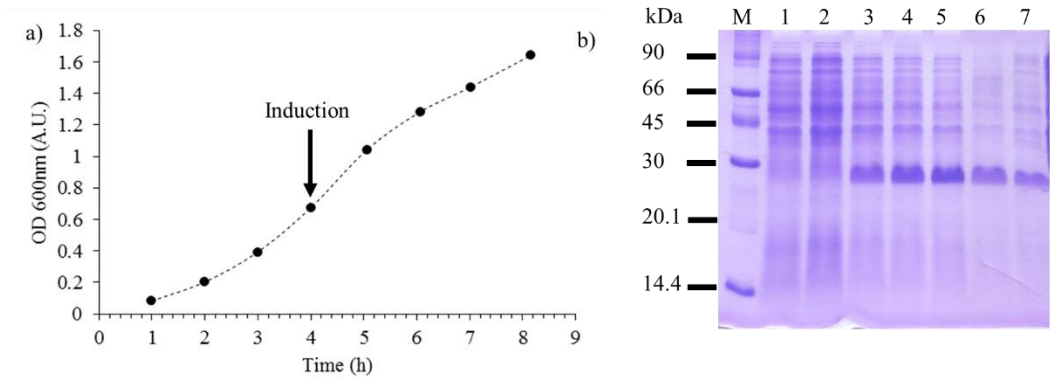

Figure 3.6: Example of a growth curve of *E. coli* BL21-DE3 (GOLD) expressing MSP1E1. The black arrow indicates the time of addition of 0.5 mM IPTG to promote the induction of protein expression, black dots indicate the measured optical density of the cells and the dashed line is a visual guideline. b) SDS-PAG of aliquots collected during *E. coli* cell growth (M –Low molecular mass marker; 1- before induction; 2- 1 hour after induction; 3- 2 hours after induction; 4- 3 hours after induction; 5- 4 hours after induction; 6- 5 hours after induction; 7- Overnight culture.

The growth of the cell culture was monitored (Figure 3.6a)) in time, and the growth profile of the transformed *E. coli* BL21-DE3 (GOLD) growing in LB medium at 37 °C was followed. The protein expression was assessed by SDS-PAGE, a protein band with higher intensity was observed, in lanes 3 to 7, which migrated close to the 30 kDa marker (Figure 3.6b)), corresponding to the expected molecular mass of the MSP1E1. The MSP1E1 band intensity remains constant after four hours of expression, suggesting that 4 hours of expression are enough to obtain MSP1E1.

After confirmation of MSP1E1's expression, cells were disrupted and the soluble fraction was obtained as described in Material and Methods. The soluble fraction was subjected to one chromatographic step.

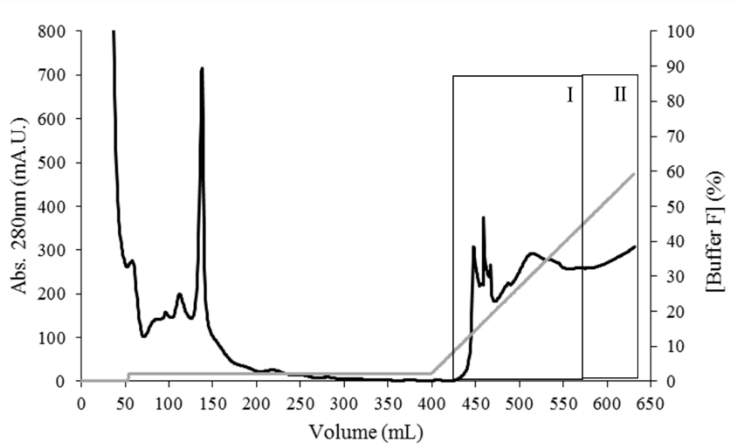

Figure 3.7: IMAC's chromatogram of MSP1E1. The black trace represents the absorbance at 280 nm and the grey line the concentration of buffer F (40 mM Tris-HCl, 300 mM NaCl, 500 mM imidazole, pH 8).

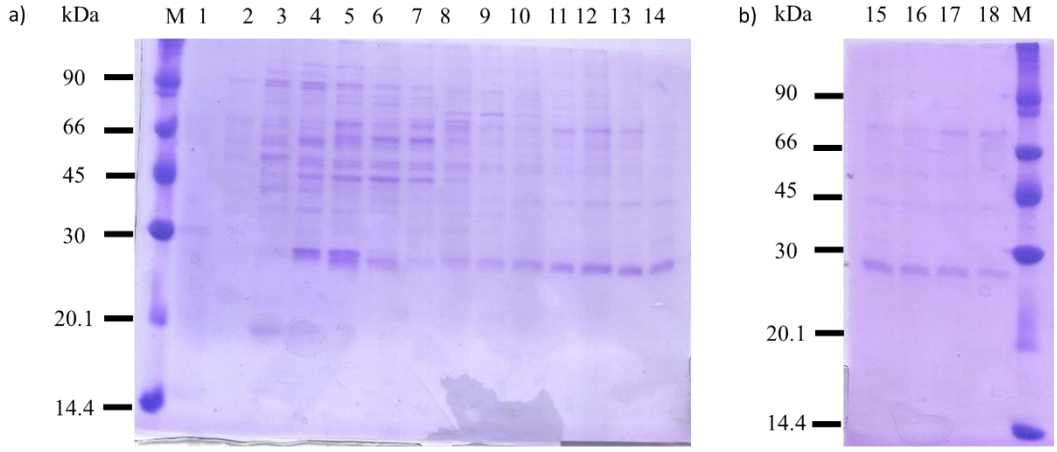

Figure 3.8: SDS-PAG of the different fractions from the IMAC chromatography. a) SDS-PAG of fraction I, M-Low molecular mass marker; 2-14 sequential tubes from fraction I. b) SDS-PAGE of fraction II 15-18 sequential tubes from fraction II, M-Low molecular mass marker.

The purification of the MSP1E1 was performed in an IMAC column. The chromatogram in Figure 3.8 shows several proteins eluting at different percentages of buffer F: at 0 % buffer F, the proteins that did not interact with the resin were eluted; increasing buffer F to 5 % lead to further elution of weakly interacting proteins; when an elution gradient from 5 % to 60 % was performed, several proteins eluted. These, correspond to proteins that strongly interacted with the resin. The presence of his tag is expected to increase the interactions with the resin, thus the elution of the MSP1E1 is expected to take place in the imidazole gradient step.

To identify where the MSP1E1 was eluted a SDS-PAGE of the different fractions was performed. The SDS-PAG (Figure 3.9) showed a band which is compatible with the molecular mass of MSP1E1 (27 kDa) in lanes 4 to 18. SDS-PAG also indicated that MSP1E1 was purified with less contaminants in samples in lanes 10 to 18. These last samples were combined and concentrated for posterior experiments. The same behavior in cell growth, protein profiles and protein purification for ^{15}N-MSP1E1 was observed.

The expression and the purification of MSP1E1 and ^{15}N-MSP1E1 were successful allowing the process of assembly of NDs and posterior characterization studies.

3.2.2 Purification of Nanodiscs

Nanodiscs were obtained by following the procedures for self-assembly as described in Materials and Methods section 2.2.3. In this thesis, two types of Nanodiscs of different lipid composition were used. One type was composed of MSP1E1 and pure POPC lipids (ND_P) and the other constituted by MSP1E1 and *E. coli* lipid (ND_E). The correctly assembled Nanodiscs were separated by one chromatographic step shown in Figure 3.10 (for POPC lipids) and Figure 3.11 (for the *E. coli* lipids).

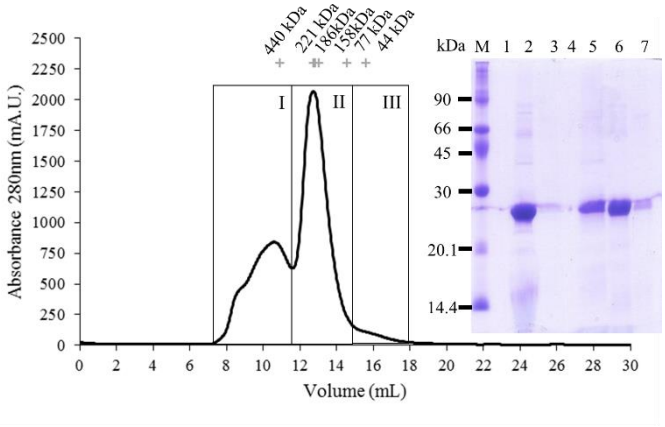

Figure 3.9: S-200 SEC's chromatogram and SDS-PAG of ND_P. In the SDS-PAG: M-Low Molecular Mass Marker; 1 – Empty lane; 2 – Before injection in S-200; 3 – Filtrate of injected sample; 4 – Empty; 5 – Fraction I; 6 – Fraction II and 7- Fraction III.

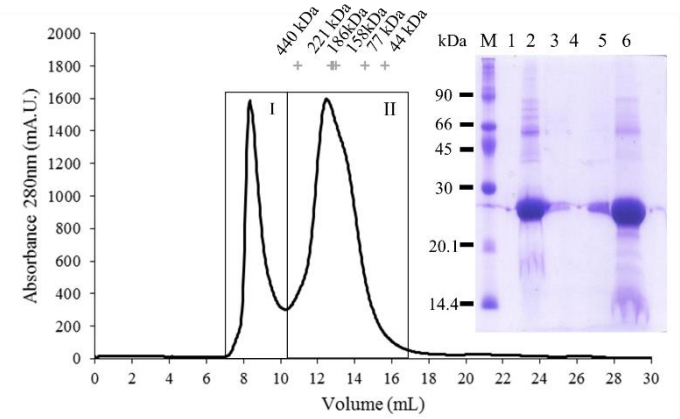

Figure 3.10: S-200 SEC's chromatogram and SDS-PAG of ND_E. In the SDS-PAG: M-Low Molecular Mass Marker; 1 – Empty lane; 2 – Before injection in S-200; 3 – Filtrate of injected sample; 4 – Empty; 5 – Fraction I; 6 – Fraction II.

Both chromatograms show the elution of different proteins complexes at different retention volumes. The SDS-PAGs represented next to the chromatograms show an intense band, which migrated close to the 30 kDa marker, confirming the presence of the MSP1E1.

The peak corresponding to the NDs with the expected size and molecular mass is close to 12.5 mL (Figure 3.9 and Figure 3.10). This elution corresponds to a Stokes' diameter of 10.3 nm, which is the

expected diameter of those NDs (see Table 1-3) and to a molecular mass near 175 kDa. The peaks present in both chromatograms are well resolved, which indicates that the separation process was efficient.

In both chromatograms, a peak at 8 mL of elution was observed, as this elution volume corresponds to the void volume of the column it was assigned to particles that have a higher molecular mass.

After the successful purification step, the NDs stored at 4 °C for further characterizations.

3.3 Biophysical characterization of Nanodiscs

Nanodiscs (ND_P and ND_E) and free MSP1E1 protein were studied by several techniques: fluorescence spectroscopy, circular dichroism, dynamic light scattering, size exclusion chromatography, UV-Visible and NMR spectroscopies.

3.3.1 Determination of the Stokes' radius and molecular mass

A size exclusion chromatography can be used to determine the hydrodynamic radius (Stokes' radius) and the molecular mass of the purified NDs, using calibration curves with standards of known Stokes' radius and molecular mass. The procedures for the determination of the Stokes' radius and for the molecular mass are described in the Material and Methods.

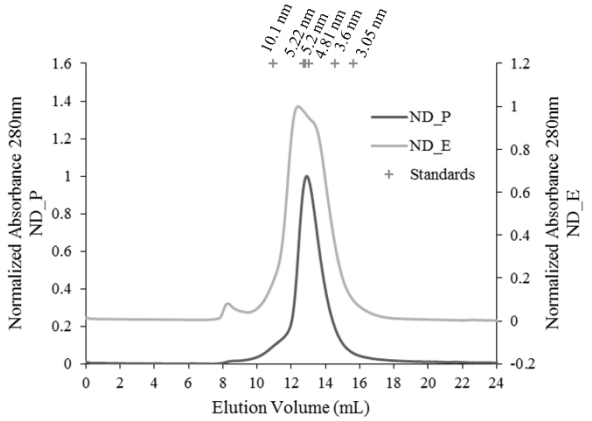

Figure 3.11: Normalized elution profiles of ND_P and ND_E in a 24 mL S-200 SEC column. The Stokes' radius, of protein standards, are also indicated above the graph.

The S-200 SEC chromatograms of ND_P and ND_E are represented in Figure 3.11 and the elution volume of both NDs was near 12.5 mL, meaning they have similar volume and molecular mass.

The Stokes' radius and molecular mass of the Nanodiscs were assessed by combining the information from the elution volumes and the Stokes' radius or molecular mass from protein standards (Figure 3.12 and Figure 3.13).

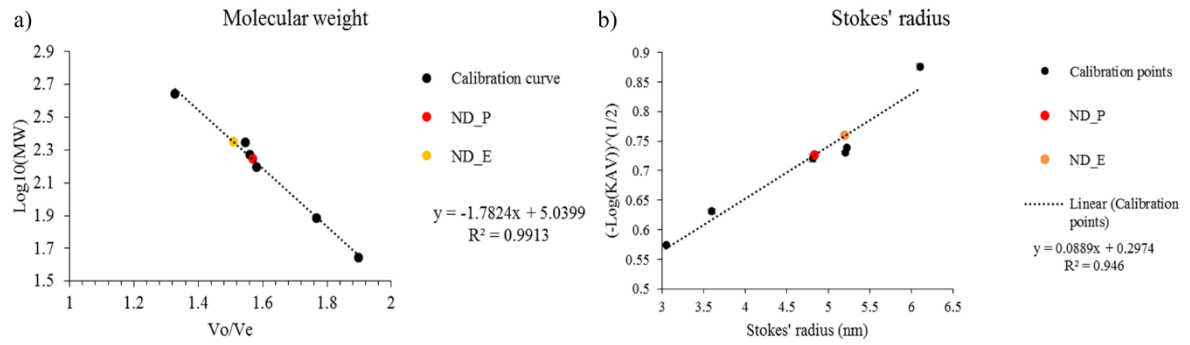

Figure 3.12: Calibration curves for the determination of: a) Stokes' radius and b) molecular mass of the NDs. The colors red and orange refer to ND_P and ND_E, respectively.

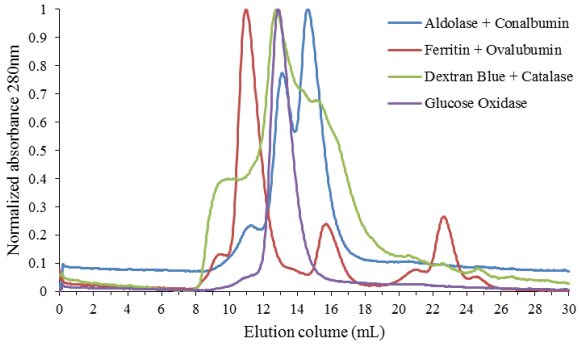

Figure 3.13: Normalized elution profile of the different proteins used for the determination of molecular mass and Stokes' radius of NDs. The standards are: Aldolase (blue), Catalase (green), Conalbumin (blue), Dextran blue (green for calibration reference), Ferritin (red), Glucose Oxidase (purple) and Ovalbumin (red).

The chromatograms represented in Figure 3.12 are the second purification of the NDs (ND_P and ND_E), therefore the identified populations of NDs will be present during the biophysical characterization.

The elution profile of ND_P (Figure 3.12 dark grey) showed the NDs elute at 12.9 mL with a small shoulder at lower elution volumes. According to literature[44], this small shoulder should correspond to NDs with different lipid/protein ratios. However, these slightly bigger NDs should not affect the further characterization of the NDs because they are present in low amount. An elution volume of 12.9 mL, according to the calibration curves (Figure 3.13) corresponds to a 4.83 nm radius and to a 175.59 kDa. These values are in agreement with the predicted molecular mass (175.34 kDa) and diameter (10.3 nm of diameter Table 1-3) for the MSP1E1 NDs.

The elution profile of ND_E (Figure 3.12 light grey) showed three peaks at 8 mL, 12.4 mL and 13.37 mL. The first elution volume corresponds to aggregates, as it elutes at the void volume of the column. This population of aggregates is small, meaning that they should not influence the biophysical characterization of the NDs. The second retention volume corresponds to NDs with 5.20 nm and 225.10 kDa. The third retention volume corresponds to 139.10 kDa and 4.5 nm. The two peaks near the expected volume are not well resolved. A possible explanation, for the existence of the two peaks, is that the stoichiometry lipid:MSP1E1 is not the correct one and the self-assembly conditions were not optimal.

ND_P and ND_E have similar retention volumes, consequently similar Stokes' radius and molecular mass. Both types of NDs were assembled at the same time and ND_E presents a small peak at 8 mL that corresponds to aggregates suggesting that the ND_E is less stable and tend to aggregate faster than ND_P.

These results show that the assembled NDs (ND_P and ND_E) have the expected characteristics thus further biophysical characterization can be performed.

3.3.2 Fluorescence spectroscopy

Fluorescence spectroscopy is a technique that can study the intrinsic fluorescence of proteins. The amino acids residues that exhibit fluorescence are tryptophan, phenylalanine, and tyrosine[75]. Using fluorescence spectroscopy it is possible to study the environment[75] (e.g. polar or apolar) in which these residues are embedded. Tryptophan residues absorb more than the other two amino acid residues, thus this residue dominates the fluorescence emission spectrum[75].

The fluorescence of the tryptophans was determined at room temperature aiming to investigate their environment when reconstituted in the NDs. The maximum intensity of fluorescence was close to 340 nm for all studied samples (Figure 3.15, Figure 3.16 and Figure 3.17). According to literature[72], this wavelength suggests the tryptophan's environment is polar, in this case, the tryptophans are exposed to the buffer.

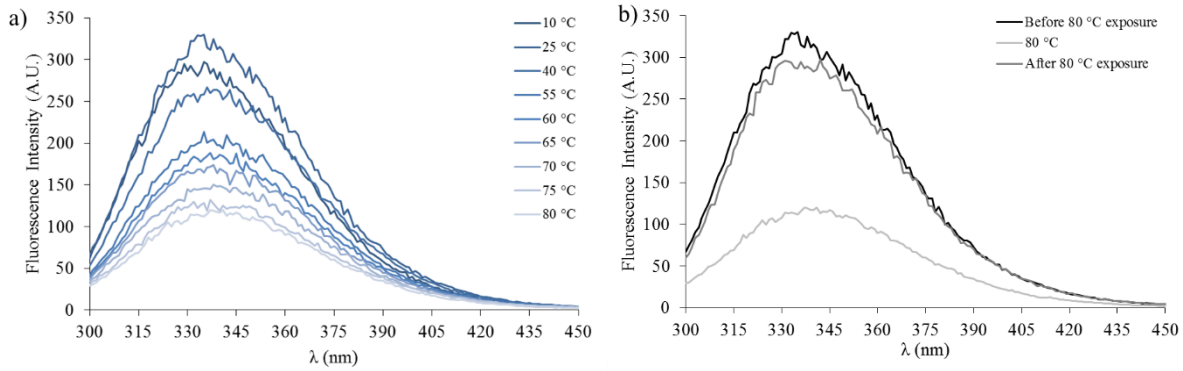

Figure 3.14: a) Fluorescence emission spectra, with excitation at 280 nm, of ND_P from 10 °C to 80 °C and b) Fluorescence emission spectra of ND_P at 25 °C (before and after being 80 °C exposure). The spectra obtained at 80 °C is shown for comparison. Samples were prepared in 50 mM Tris-HCl, 300 mM NaCl pH 8.

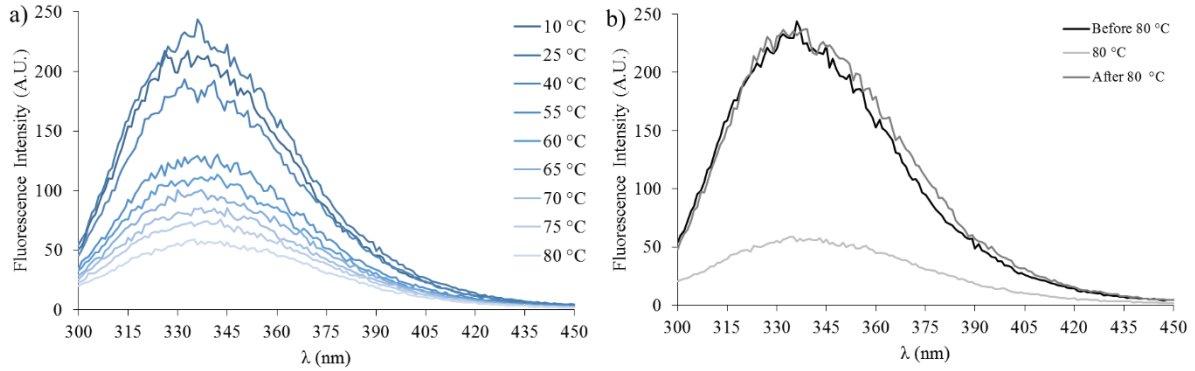

Figure 3.15: a) Fluorescence emission spectra, with of excitation at 280 nm, of ND_E from 10 °C to 80 °C and b) Fluorescence emission spectra of ND_E at 25 °C (before and after being 80 °C exposure) and at 80 °C. The spectrum obtained at 80 °C is shown for comparison. Samples were prepared in 50 mM Tris-HCl, 300 mM NaCl pH 8.

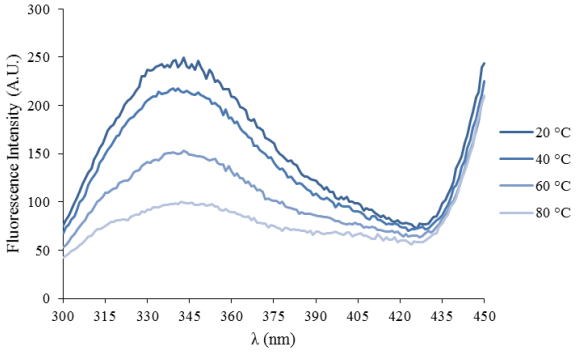

Figure 3.16: Fluorescence emission spectra of isolated MSP1E1, with excitation at 280 nm, from 20 °C to 80 °C. Samples were prepared in 50 mM Tris-HCl, 300 mM NaCl pH 8.

Fluorescence emission spectra obtained at different temperatures for NDs and of MSP1E1 (Figure 3.14 a), Figure 3.15 a) and Figure 3.16) show that the band maximum wavelength remains at 340 nm. This indicates that the tryptophans do not change their environment (i.e. polar) at the studied temperatures.

With increasing temperature, it was also observed the decrease of fluorescence intensity. This occurs due to the decrease of the tryptophans' excitation lifetime, where the energy from tryptophans' excited state is transferred to the solvent[76].

A thermal stability test was made to assess the behavior of NDs after exposure to 80 °C as described in the Materials and methods. Figure 3.14b) and Figure 3.15b) show the spectra for both types of NDs at 20 °C, before and after exposure to 80 °C, and at 80 °C. The NDs present similar spectra before and after exposure to 80 °C, suggesting the fluorescence intensity recovers and that NDs are stable at the studied temperatures.

The changes in the tryptophans' fluorescence intensity was assessed by plotting the normalized fluorescence intensity values at 340 nm as function of temperature (Figure 3.17a)). Normalization was calculated by determining the highest fluorescence value at 340 nm, from the different samples, and performing a division of all values by the highest fluorescence value. For the NDs, the values at 340 nm were extracted from Figure 3.14 a) and Figure 3.15 a) and plotted as a function of temperature.

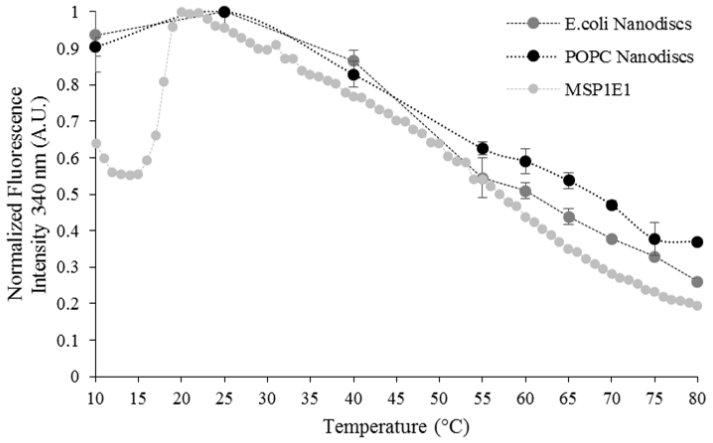

Figure 3.17: Normalized fluorescence intensity at 340 nm for the different NDs and for MSP1E1 in solution as a function of temperature. Dots represent the calculated values and the lines are visual guidelines.

Analyzing Figure 3.17, the fluorescence intensity of free MSP1E1 increases from 0.64 to 1 from temperatures ranging from 10 to 20 °C. For the NDs samples, the fluorescence intensity increases from 0.9 to 1. Afterwards, a linear decrease in the fluorescence intensity at 340 nm is observed, for all samples, until 80 °C. The linear decrease of the fluorescence intensity of tryptophans indicates that a transition is not occurring and only the tryptophans' excitation lifetime is affecting the fluorescence intensity.

During the temperature dependent experiments for the NDs samples, precipitate in the cell walls was observed after 40 °C measurements. This suggested the NDs could precipitate with the increase of temperature. However, the fluorescence values returned to its initial values, meaning that the same amount of protein is emitting fluorescence. This leads to a hypothesis were the lipids precipitate and the MSP1E1 remain in solution.

The fluorescence assays show the tryptophans, present in the MSP1E1, are exposed to the buffer and the fluorescence intensity is not affected after an exposure to 80 °C. This suggests the MSP1E1 in the NDs are stable.

3.3.3 Circular dichroism

Circular dichroism allows studying the secondary structure of proteins by measuring the difference of absorbed polarized light. In this study, circular dichroism assessed the secondary structure of MSP1E1 in solution and in NDs. CD spectra for the different samples were collected at different temperatures, ranging from 10 °c to 80°C, to assess the variations of secondary structure with the temperature as described in Materials and Methods.

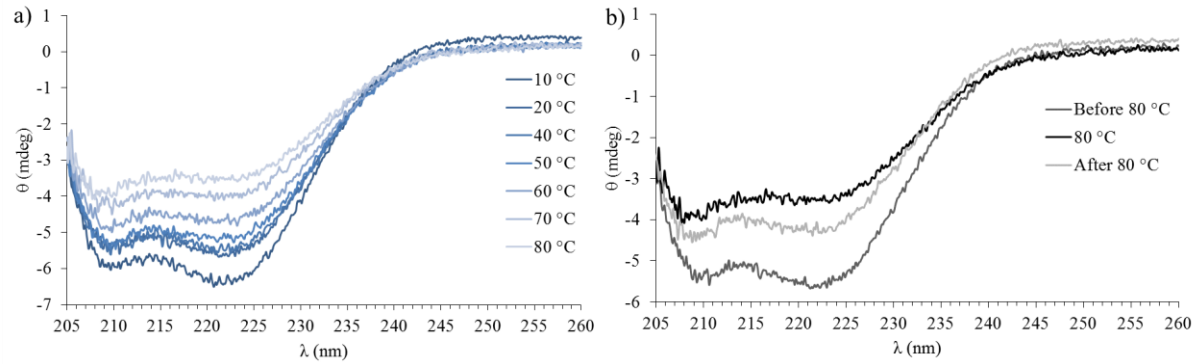

Figure 3.18: a) Circular dichroism spectra of ND_P at different temperatures from 10 °C to 80 °C and b) circular dichroism spectra of ND_P at 20 °C, before and after 80 °C exposure. The spectra obtained at 80 °C is shown for comparison. Samples were prepared in 50 mM Tris-HCl, 300 mM NaCl pH 8.

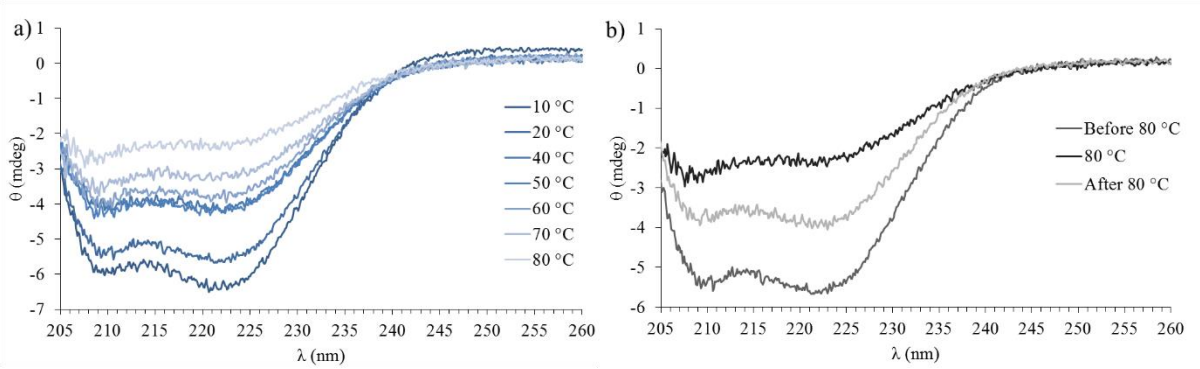

Figure 3.19: a) Circular dichroism spectra of ND_E at different temperatures from 10 °C to 80 °C and b) circular dichroism spectra of ND_E at 20 °C, before and after 80 °C exposure. The spectra obtained at 80 °C is shown for comparison. Samples were prepared in 50 mM Tris-HCl, 300 mM NaCl pH 8.

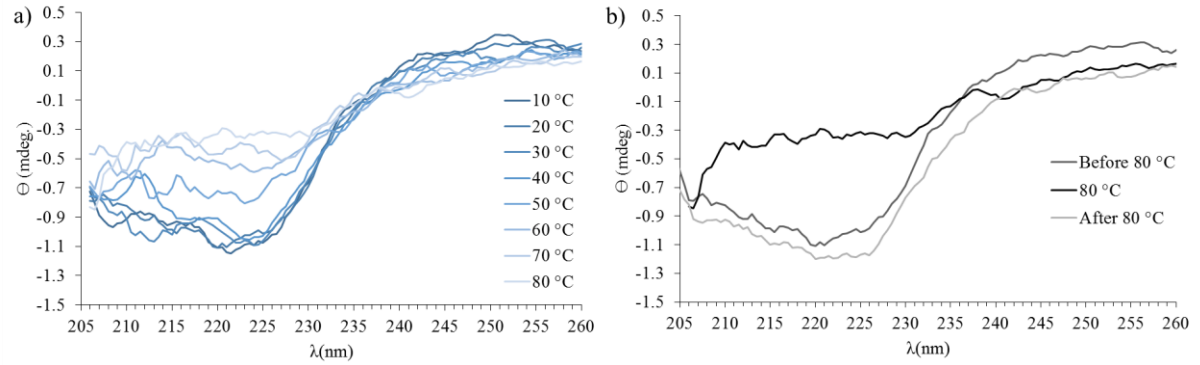

Figure 3.20: a) Circular dichroism spectra of MSP1E1 at different temperatures from 10 °C to 80 °C and b) circular dichroism spectra of MSP1E1 at 20 °C, before and after 80 °C exposure. The spectra obtained at 80 °C is shown for comparison. Samples were prepared in 50 mM Tris-HCl, 300 mM NaCl pH 8.

CD spectra for the MSP1E1 in solution and in the NDs have a similar shape (see Figure 3.18 a), Figure 3.19 a) and Figure 3.20 a)), presenting two minima at 208 nm and 222 nm. These spectra are characteristic of a protein having an α-helix secondary structure[77].

Increasing the temperature leads to a loss of signal, suggesting there is a loss of secondary structure. In addition, with increasing temperature the shape of the spectra still maintains α-helical typical shape. This indicates a loss in the α-helix content without a transition to another type of secondary structure and it is possible that the structure of the MSP1E1 is becoming unordered. A thermal stability test was performed to assess if the secondary structure of MSP1E1 returns to the initial value after being exposed to 80 °C. For MSP1E1 in solution (Figure 3.20 b)) the CD spectra are similar before and after exposure to 80 °C, indicating that the MSP1E1 can recover its secondary structure after exposure to 80 °C. For the MSP1E1 of ND_P and ND_E (Figure 3.18b) and Figure 3.19b)) there is not a total recovery of its structure, because the spectra after exposure to 80 °C does not overlap with the spectrum at 20 °C. The spectra of ND_P and ND_E, after exposure to 80 °C, is similar to the spectra at 70 °C and to 60 °C, respectively.

The ellipticity at 222 nm reflects the α-helix content, thus it was plotted as function of temperature.

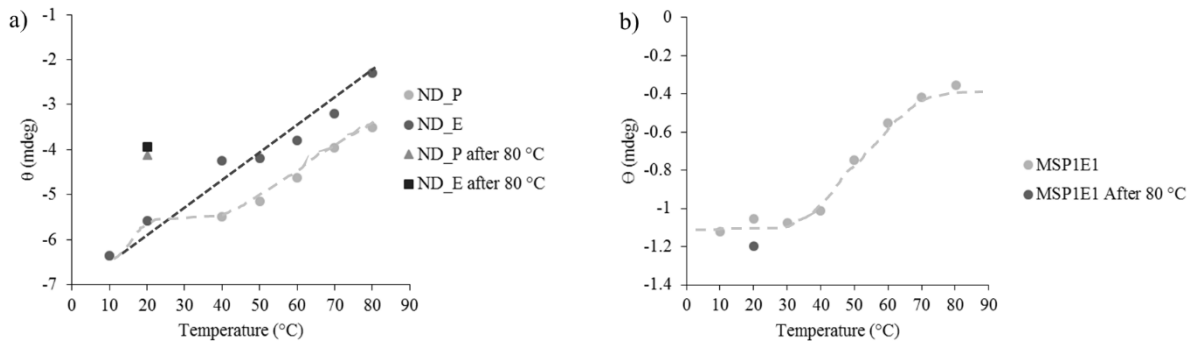

Figure 3.21: Circular dichroism ellipticity at 222 nm for the different NDs and for MSP1E1 in solution as a function of temperature. The dashed lines are visual guidelines.

Figure 3.21 a) and b) shows the increase of the ellipticity at 222 nm for the NDs and for the free MSP1E1, respectively, with the increase of temperature. For free MSP1E1 it increases slightly from 10 °C to 40 °C and then increases further until it reaches 80 °C. For ND_P the ellipticity at 222 nm rise from 10 °C to 20 °C, remains almost constant until 40 °C and then increase until 80 °C. For *E. coli* lipid NDs, the ellipticity 222 nm rise from 10 °C to 80 °C almost linearly. This means that the free MSP1E1 and the MSP1E1 in NDs are losing its α-helix structure. Since the values of the curve at 222 nm are different, then the loss of α-helix structure must be different.

These observations suggest the α-helix secondary structure is lost in a different manner for free MSP1E1 and for MSP1E1 in NDs.

3.3.4 Dynamic Light Scattering

Dynamic light scattering (DLS) is a technique that allow the calculation of the size of a particle through light dispersion, assuming the particle is a sphere. In this work, we are interested in calculating the diameter of the NDs. Due to its shape, the average rotation of NDs in solution will average out as a sphere, thus allowing to use this approximation.

The diameter for the different NDs, ND_P and ND_E, was assessed at different temperatures, ranging from 10 °C to 80 °C, as described in Materials and Methods.

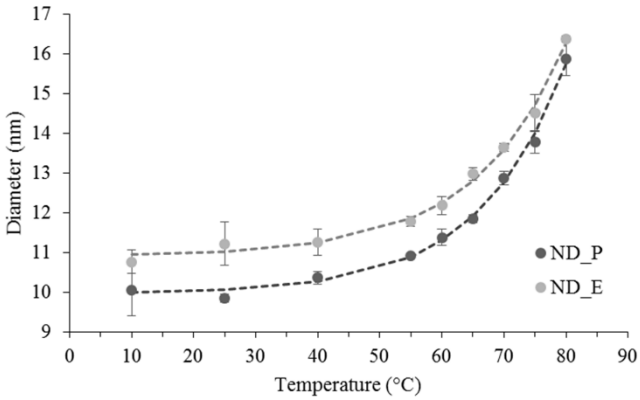

Figure 3.22: Diameter of the different NDs as a function of temperature obtained by dynamic light scattering. The dashed lines are visual guidelines. Samples were prepared in 50 mM Tris-HCl, 300 mM NaCl pH 8.

Figure 3.22 shows the diameter variation of the NDs with increasing temperature from 10 to 80 °C. Both types of NDs become larger as the temperature increases and the ND_E presents a higher diameter that ND_P at the studied temperatures.

At 10 °C, ND_P have a 10.1 ± 0.7 nm in diameter and the diameter slightly decreases at 25 °C. However, the measurement at 10 °C has a higher associated error than that performed at 25 °C. After 25 °C, the diameter increases almost 1 nm until 55 °C. At this point, the diameter begins to rise in an exponential way until 15.9 ± 0.4 nm at 80 °C. ND_E at 10 °C have a diameter of 10.7 ± 0.3 nm and the diameter almost remains constant until 40 °C. After this point, the diameter increases almost 1 nm from 55 °C to 65 °C. From 65 °C to 80 °C, the diameter of NDs raises in an exponential way to 16.4 ± 0.1 nm.

Considering the measurements at 10 °C as a reference of the NDs (e.g. 100%) then at 80 °C the diameter of the ND_P increased 152 % and that of ND_E increased 158 %. The increase in diameter can be related with increase of molecular vibrations of the lipids in the NDs as well the loss of secondary structure of the MSP1E1.

3.3.5 UV-Visible spectroscopy

In the previous characterization approaches, precipitation in the cuvettes walls was observed when heating the NDs samples above 40 °C, while the solution remained clear.

In order to understand whether NDs precipitate, the absorbance of NDs at 280 nm was monitored as described in Materials and Methods. If the absorbance at 280 nm of the MSP1E1 decreases, then the amount of protein in solution decreases, suggesting the precipitation of NDs.

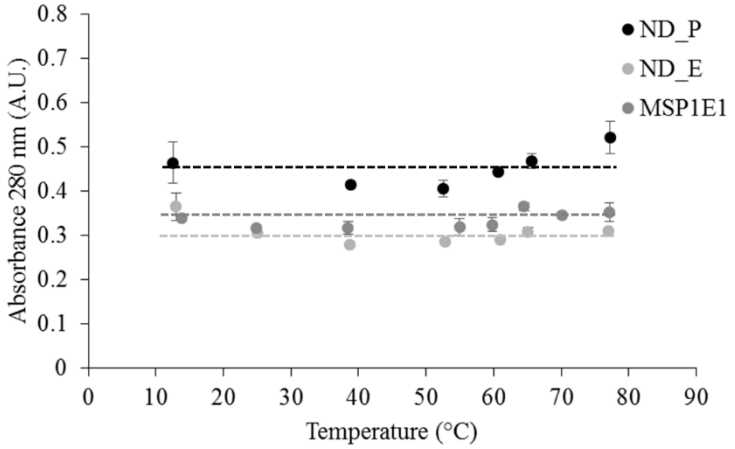

Figure 3.23: UV-Visible absorbance values at 280 nm for MSP1E1 and the different types of NDs plotted as function of the temperature. Dashed lines are visual guidelines. Samples were prepared in 50 mM Tris-HCl, 300 mM NaCl pH 8.

The absorbance at 280 nm of the different samples is show in Figure 3.23. The obtained absorbance, at different temperature for all samples, show that the variation of absorbance within the studied temperatures is not significant. In addition, during the measurements of free MSP1E1 there were not observed any precipitates.

These observations suggest that the MSP1E1 does not precipitate when heated to 80 °C and that the precipitates from the temperature dependent experiments are most probably lipids.

3.3.6 Nuclear Magnetic Resonance spectroscopy

NMR spectroscopy is a powerful technique that allows the study of the electromagnetic proprieties of nucleus. This spectroscopy was used to fingerprint the lipids and to understand how they behave at different temperatures.

In this work, NMR spectroscopy experiments such as: heteronuclear single quantum coherence spectroscopy (HSQC) and ^{31}P were used to characterize Nanodiscs.

3.3.6.1 NMR of MSP1E1

NMR experiments of free MSP1E1 were performed as a control as well to assign resonances in the NMR spectra of NDs.

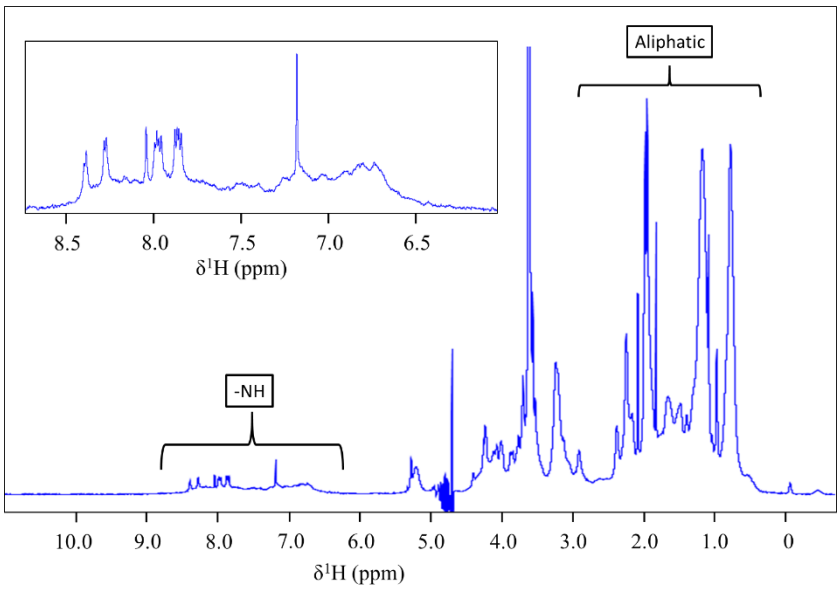

Figure 3.24: ^{1}H NMR spectrum of MSP1E1 at 15 °C (50 mM NaH_2PO_4, 300 mM of NaCl, pH 7.5). The inset shows the region from 6 to 9 ppm.

The 1D ^{1}H-NMR spectrum (see Figure 3.24) shows all hydrogens in solution, with the exception of those provided by the solvent, whose signal was suppressed. Resonances between 0 ppm and 2.5 ppm correspond to the aliphatic groups, present in the amino acid residues of MSP1E1. The resonance with a high intensity near 4 ppm is a contribution of CH groups from different sources, including the Tris-HCl buffer, which remained from purification and even after buffer exchange, and the α-carbons of MSP1E1.

The region between 6 ppm and 8.5 ppm presents signals with lower intensities, corresponding to the backbone and to aromatic -NH groups. The resonances of the spectrum between 6 to 8.5 ppm (inset in Figure 3.24) are disperse, indicating the protein has a defined structure, which agrees with the CD results that showed MSP1E1 has a α-helical secondary structure.

The HSQC NMR experiment is a two-dimensional heteronuclear methodology that correlates two different nuclei that are connected by one covalent bond. In the NDs system, ^{1}H-^{13}C HSQC spectrum

shows the resonances of the MSPs and of the lipids. The lipids present in the NDs are highly concentrated (in the order of the mM) allowing measurements of ^{13}C nuclei in their natural abundance. In addition, due to MSP:lipid ratio (see Table 1-4), the lipids' resonances will be more intense than the MSP1E1's resonances.

Different NMR experiments, such as ^{1}H-^{13}C HSQC and ^{1}H-^{15}N HSQC, were performed for free MSP1E1 that served as controls for future assignment. The ^{1}H-^{13}C HSQC spectrum can be used to assign resonances from the MSP1E1 in the NDs' ^{1}H-^{13}C HSQC NMR spectrum. The ^{1}H-^{15}N HSQC spectrum, provides the MSP1E1 fingerprint free in solution. Since the nuclei are sensitive to the electromagnetic environment ^{1}H-^{15}N NMR experiments can be used to assess the behavior of the MSP1E1 residues in different buffers.

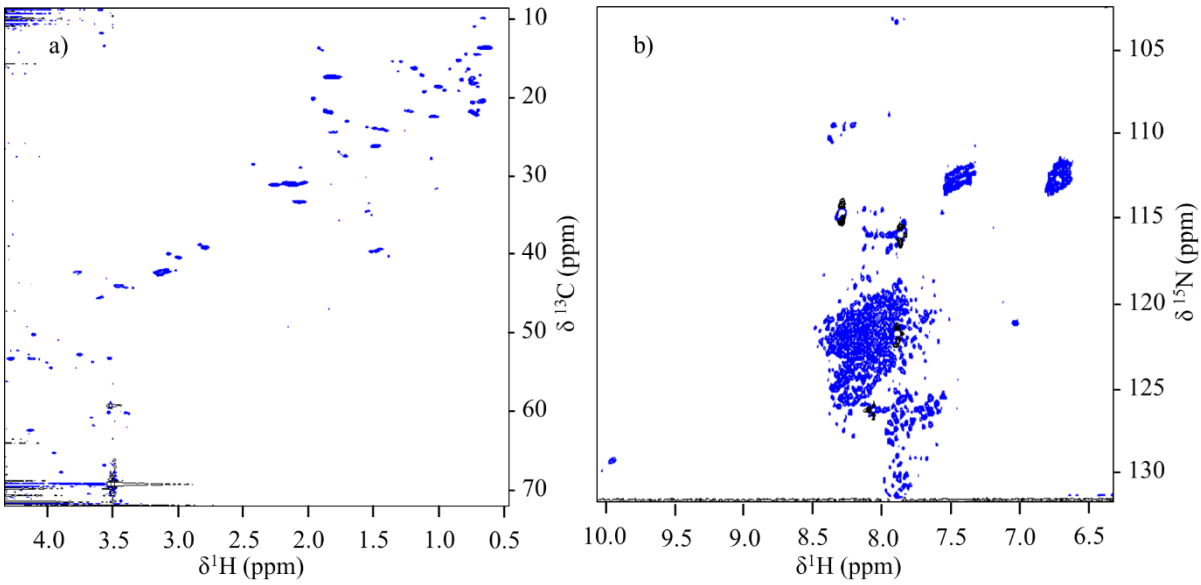

Figure 3.25: ^{1}H-^{13}C HSQC NMR spectrum of MSP1E1 using ^{13}C's natural abundance at 15 °C (50 mM NaH_2PO_4, 300 mM NaCl pH 8). b) ^{1}H – ^{15}N HSQC spectrum of ^{15}N labeled MSP1E1 at 15 °C (50 mM NaH_2PO_4, 300 mM NaCl pH 8). The estimated concentration of ^{15}N labeled MSP1E1 is 413 µM by the absorbance of MSP1E1 at 280 nm.

The Figure 3.25 shows NMR spectra of free MSP1E1 in solution. The ^{1}H-^{13}C HSQC spectrum (Figure 3.25 a)) shows the correlation between hydrogens covalently bonded to carbons from different CH_n present in MSP1E1. These resonances range from 0.5 ppm to 4.5 ppm in ^{1}H axis and from 10 ppm to 70 ppm in the ^{13}C axis.

The Figure 3.25b) shows the resonances of hydrogen covalently bonded to nitrogen, from amino acid residues backbone and side chain. The ^{1}H-^{15}N HSQC spectrum shows a dispersion of resonances ranging from 105 ppm and 135 ppm ^{15}N axis and from 6.5 ppm to 10 ppm in ^{1}H axis.

3.3.6.2 ^{1}H-^{13}C HSQC NMR experiments of NDs

The ^{1}H-^{13}C HSQC NMR experiments were performed as described in Materials and Methods. These experiments were aimed to obtain spectra for ND_P and ND_E in order to assign the lipid chain resonances from the NDs.

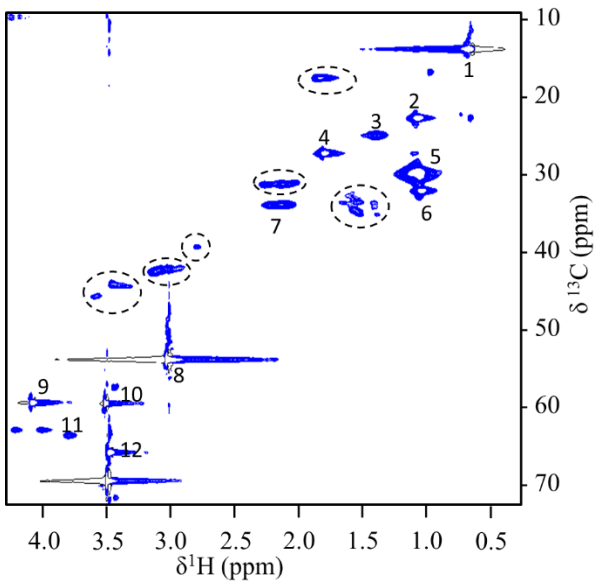

Figure 3.26: ^{1}H-^{13}C HSQC spectrum of ND_P at 15 °C (50 mM NaH_2PO_4, 200 mM NaCl pH 7.5). The estimated concentration of NDs is 160 µM by the absorbance of ND_P at 280 nm. The numbers represent the chemical groups represented in Figure 3.28 and the dashed circles represent the resonances corresponding to MSP1E1.

The ^{1}H-^{13}C HSQC spectrum of ND_P (see Figure 3.26) shows the resonances between 0.5 ppm and 4.5 ppm of ^{1}H axis and between 10 ppm to 70 ppm of ^{13}C axis. This spectrum shows the correlation between the hydrogens covalently bonded to carbon in the different CH_n groups, which are present in lipids and in MSP1E1's amino acid residues. Resonances in the ^{1}H-^{13}C HSQC spectrum were assigned based on existing literature[51] of POPC NDs (see numeration near resonances in Figure 3.26 and respective chemical group in Figure 3.27). To assign the resonances from the MSP1E1 in ND_P, the spectrum of MSP1E1 was superimposed with ^{1}H-^{13}C HSQC spectrum of ND_P.

In Figure 3.27, there are resonances whose assignment is not clear.

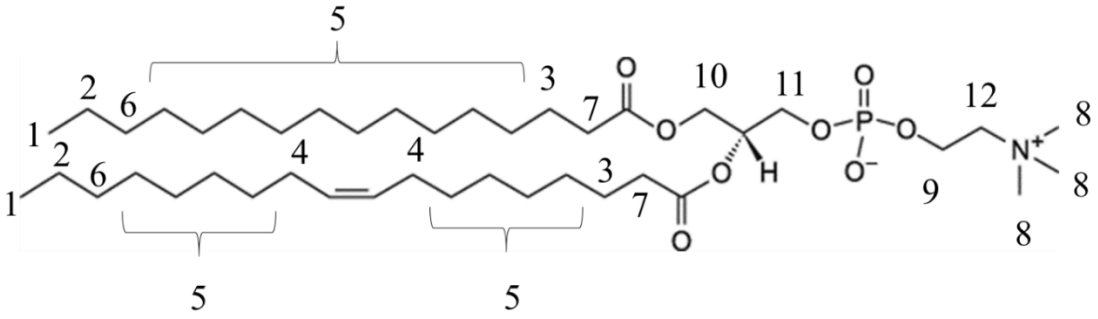

Figure 3.27: Schematic representation of POPC lipid. Numbers represent the peak ID in Table 3-2 identify the carbons and protons.

Table 3-2: ^{1}H and ^{13}C chemical shifts of ND_P at 15 °C. Peak assignment of ND_P was based on published assignment for POPC[51] NDs and in ^{1}H-^{13}C HSQC MSP1E1 NMR spectra.

^{1}H chemical shift (ppm)	**^{13}C chemical shift (ppm)**	**Peak ID**	**Carbon(s)**
0.6699	13.7	1	-**C**H_3
0.959	16.81		
1.831	17.61	MSP1E1	
0.7301	22.33		
0.6538	22.63		
1.059	22.73	2	-**C**H2-CH_3
1.084	23.44		
1.37	24.84	3	-OCO-CH_2-**C**H_2-
1.092	27.25		
1.786	27.55	4	-**C**H_2-C=
1.063	29.76	5	-$(CH_2)_n$
2.05	31.02	MSP1E1	
2.119	31.17	MSP1E1	
2.258	31.24	MSP1E1	
1.027	32.17	6	-**C**H_2-CH_2-CH_3
1.569	33.68	MSP1E1	
2.132	33.82	7	-OCO-**C**H_2-
2.208	33.87	7	-OCO-**C**H_2-
1.409	33.85	MSP1E1	
2.794	39.25	MSP1E1	
2.938	42.02	MSP1E1	
3.014	42.17	MSP1E1	
3.107	42.39	MSP1E1	
3.449	44.18	MSP1E1	
3.582	45.62	MSP1E1	
3.027	53.88	8	-N^+-(**C**H_3)$_3$
3.499	56.99		
3.436	57.38		
4.086	59.37	9	-O-**C**H_2-CH_2-
3.508	59.5	MSP1E1	
3.482	61.4		
4.208	62.84		
4.005	62.86		
3.794	63.6	11	-CH_2-OP(Glycerol)
3.476	65.84	10	-O-CH_2-**C**HO-
3.492	69.43	12	-**C**H_2-N^+-
3.425	71.62		

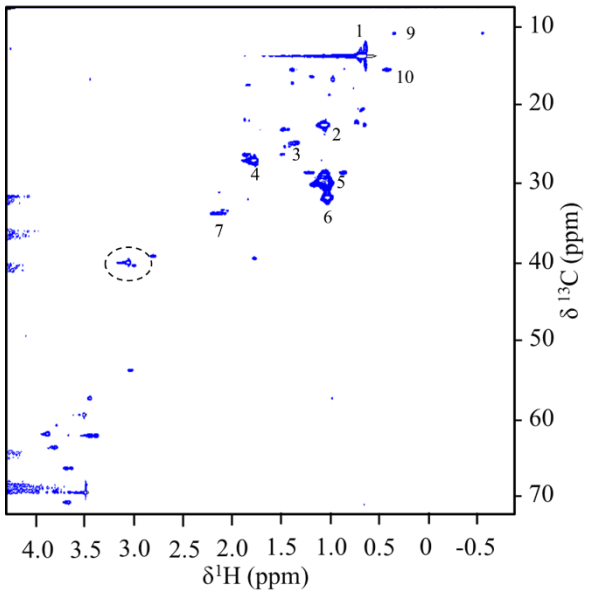

Figure 3.28: ^{1}H-^{13}C HSQC spectrum of ND_E at 15 °C (40 mM NaH_2PO_4, 200 mM NaCl pH 7.5). The estimated concentration of NDs is 101 µM by the absorbance of ND_E at 280 nm. The numbers represent the chemical groups of the phospholipids and the dashed circles correspond to the MSP1E1.

The ^{1}H-^{13}C HSQC spectrum of ND_E is represented in Figure 3.28 and it shows the acquired resonances between -1 ppm and 4.5 ppm of ^{1}H axis and between 10 ppm to 70 ppm of ^{13}C axis. The lipidic composition of ND_E and ND_P is different, thus it is expected the ^{1}H-^{13}C HSQC NMR spectrum presents differences in the chemical shift and peak pattern (Figure 3.26). The resonances for ND_E are not assigned in literature, thus, to obtain an initial assignment the ^{1}H-^{13}C HSQC spectra of ND_P, ND_E and MSP1E1 were compared. The superimposition of both NDs NMR spectra shows that they have some similar resonances, e.g. from the aliphatic groups such as -CH_3, -CH_2 and –CH. With this, it is possible to assign the resonances from chemical groups 1 to 7 (see Figure 3.28 numbered resonances). Moreover the comparison with the MSP1E1 also allowed the assignment of the resonances from MSP1E1 (see Figure 3.28 dashed circles). Based on a web application (*nmrdb*), that computes an assignment based on the molecular structure, it was possible to assign extra resonances (see Figure 6.1, Figure 6.2 and Figure 6.3) in the spectrum of ND_E. These resonances are from the cyclopropane, which is present in PE and CA lipids (Figure 1.8).

Several resonances present in the ^{1}H-^{13}C HSQC spectrum of ND_E were not assigned, however these resonances should belong to the *E. coli* lipids. The assignment of the remaining resonances from ND_E can be performed by comparison of NMR spectra of NDs with pure individual *E. coli* lipids.

Table 3-3: ^{1}H and ^{13}C chemical shifts of ND_E at 15 °C. Peak assignment of ND_E was based on published assignment for POPC[51] and in ^{1}H-^{13}C HSQC MSP1E1 spectra.

^{1}H chemical shift (ppm)	**^{13}C chemical shift (ppm)**	**Peak ID**	**Carbon(s)**	**^{1}H chemical shift (ppm)**	**^{13}C chemical shift (ppm)**	**Peak ID**	**Carbon(s)**
-0.554	10.84			1.087	29.6		
0.3455	10.84	9	-CH_2-**C**H-**C**H-CH_2	1.034	30.04		
0.6675	13.81	1	-**C**H_3	2.134	31.18	4	-**C**H_2-C=
0.4172	15.51	10	-CH_2-CH-CH-CH_2- \ / **C**H_2	1.028	31.86	6	-**C**H_2-CH_2-CH_3
1.386	15.52			1.839	32.16		
1.19	16.36			2.044	33.47		
0.9769	16.73			2.094	33.5		
1.387	17.25			2.075	33.83	7	-OCO-**C**H_2-
1.839	17.47			2.107	33.84	7	-OCO-**C**H_2-
1.01	18.7			2.198	33.84	7	-OCO-**C**H_2-
0.6663	20.55			2.804	39.3		
1.871	21.85			1.776	39.6		
1.826	21.99			3.057	40.15		
0.7281	22.16			3.002	40.56		
0.6504	22.55			3.03	53.84		
1.056	22.58	2	-**C**H2-CH_3	3.453	57.42		
1.479	23.12			3.511	59.53		
1.43	23.14			3.792	60.87		
1.34	24.84	3	-OCO-CH_2-**C**H_2-	3.886	61.95		
1.417	25.28			3.67	62.15		
1.464	25.33			3.451	62.18		
1.871	26.3			3.39	62.19		
1.486	26.31			3.813	63.69		
1.775	27.06			3.639	66.37		
0.8613	28.03			3.701	66.37		
1.224	28.62			3.498	69.53		
1.057	28.91	5	-$(CH_2)_n$	3.673	70.67		

The obtained ^{1}H-^{13}C HSQC NMR spectra will serve as a control to identify the resonances that belong to the lipids and to MSP1E1. In NDs with a reconstituted protein, these will allow to separate the resonances that belong to the reconstituted protein from the MSP.

3.3.6.3 ^{31}P NMR spectroscopy of Nanodiscs

The lipid environment of biomembranes can be studied by one dimension ^{31}P NMR spectroscopy. This type of NMR experiment provides information on the electromagnetic environment of phosphorus atom located in the polar head of the phospholipids (Figure 1.7 and Figure 1.8).

The ^{31}P NMR spectra may give information on phase transition[78] of lipids and on their interaction with proteins[79]. Studies of bicelle temperature dependence measured by ^{31}P NMR spectroscopy showed that the bicelle structure is temperature dependent. This study revealed in experiments where the lipid phase transition is reached the chemical shift of the phosphate group presents a sigmoid behavior as function of temperature[78].

In this work, the ^{31}P NMR spectroscopy was used to study the behavior of the phosphate groups, of the phospholipids in the NDs, and to identify possible transition temperatures of the *E. coli* lipids. To achieve this objective, sequential ^{31}P NMR spectra were acquired at different temperature (i.e. from 5 ° to 65 °C). Furthermore, the stability of the NDs after 65 °C was checked via the measurement at lower temperatures. For ND_P the transition temperature of POPC is at -4 °C, therefore it was not expected a transition temperature at the studied temperatures. For *E. coli* lipid extract NDs, the transition temperatures of this complex mixture of lipids are not known.

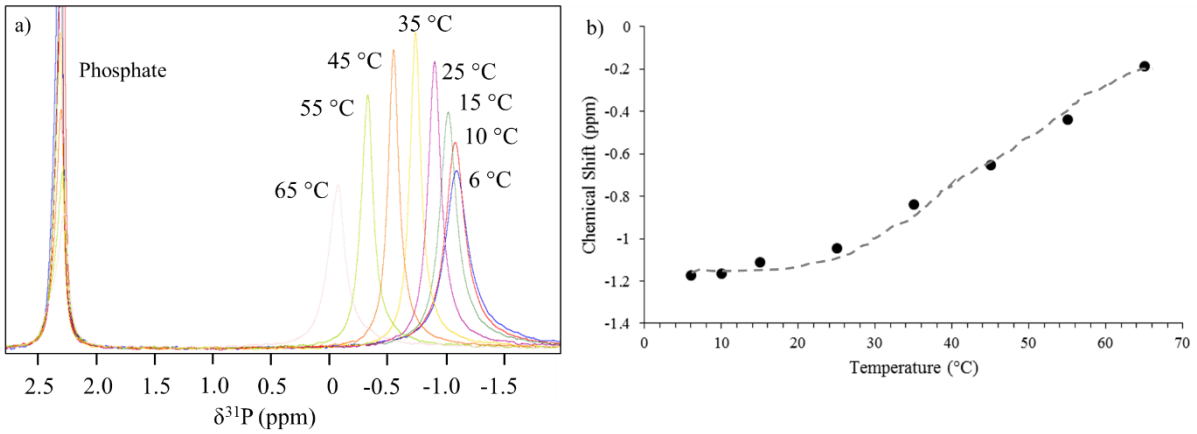

Figure 3.29: a) ^{31}P NMR spectra of ND_P obtained at different temperatures (10 mM NaH_2PO_4. 40 mM Tris-HCl, 300 mM NaCl titrated to pH 8) as described in Material and Methods. The estimated concentration of ND_P is 133.2 µM measured by absorbance at 280 nm; b) plot of chemical shift resonances as a function of temperature for the ND_P. Dots represent the measured values and dashed lines correspond to visual guidelines.

The ND_P contains only one type of lipid (the POPC, which contains a single phosphate group) thus the ^{31}P NMR spectra exhibits a unique peak, as it can be seen in Figure 3.29a). Figure 3.29a) shows that POPC's chemical shift changes to higher frequencies with increasing temperature. To help with the interpretation of the different spectra the resonance from the phosphate buffer was used as a reference (e.g. resonances from phosphate buffer were aligned at the same chemical shift). Using the internal reference the changes of the POPC lipids are related to the effects of the temperature on the NDs. Figure 3.29b) shows the chemical shift of POPC phosphorus as a function of temperature. The change in the

electromagnetic environment of the ND_P's phosphate group can be related with the increase in diameter of the NDs, as observed by DLS measurements.

Analyzing Figure 3.29a), other parameters can be obtained, such as the intensity of the peak, the linewidth and the integral. Changes in these parameters mean that there is a change in dynamics. These dynamics can be several kinds of motions of the NDs or the rotation of the phosphorous group head. In Figure 3.30a), it is visible that the intensity of the POPC's resonance increases until 35 °C and then decreases until 65 °C. The peak linewidth and the area, were plotted as a function of temperature and are shown in Figure 3.30a) and Figure 3.30b).

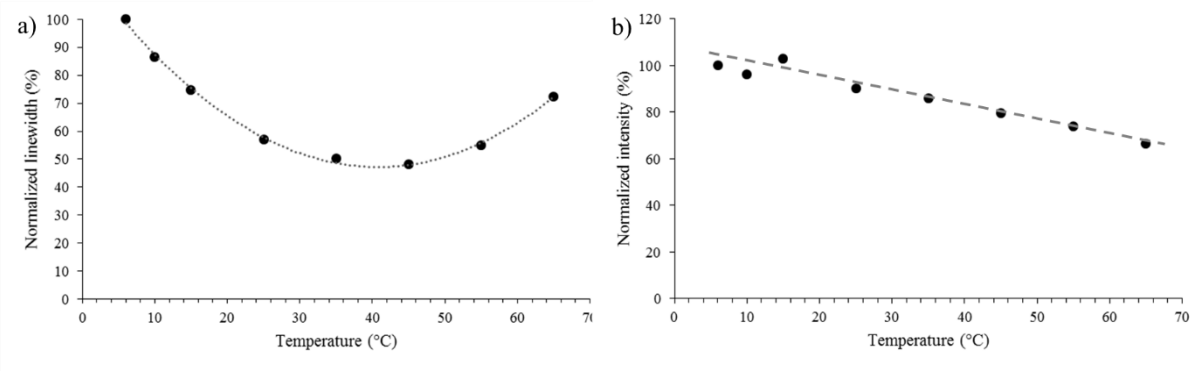

Figure 3.30: Representation of: a) normalized linewidth of peaks from POPC in the ^{31}P NMR ND_P spectra as a function of temperature; b) normalized integral of POPC's resonance as a function of temperature. Dots represent the acquired values (linewidth and integral) and dashed lines correspond to visual guidelines.

The POPC's linewidth and area were plotted as function of temperature and both of these values were normalized to the 6 °C measurement. In Figure 3.30a) the normalized linewidth decreases from 100 % (6 °C) to almost 48 % (45 °C) and then increases to almost 73 % (65 °C). In Figure 3.30b) the normalized area of the resonances linearly decreases to 66 % at 65 °C. A change in the area of the resonance indicates that there is a change in the amount of phosphorous in solution (e.g. precipitation). Aside from precipitation, which begins to occur at 40 °C, the decrease of the integral can be related with the relaxation time of the phosphorus. In addition, the relaxation time can also affect the linewidth and the integral. The relaxation time of ND_P was measured to determine if it is responsible for the variations of the phosphorous' linewidth, integral and intensity. However, the experiments' results were inconclusive.

In order to assess the stability of the NDs to temperature, the NMR spectra of ND_P sample were measured in a temperature cycle: initially at 15 °C, heated to 50 °C, afterwards cooled to 15 °C, and finally reheated to 50 °C (as described in Figure 3.31).

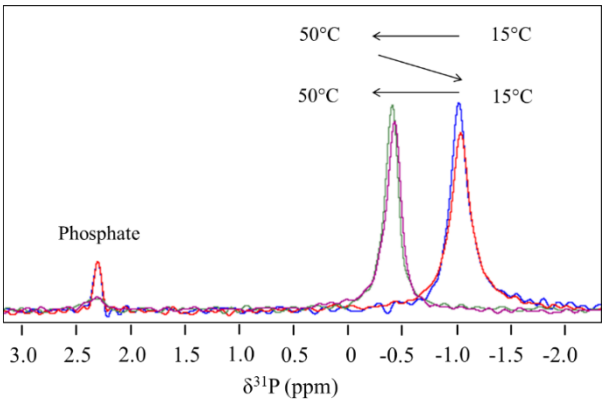

Figure 3.31: ^{31}P NMR spectra of ND_P obtained at different temperatures (1 mM NaH_2PO_4. 40 mM Tris-HCl, 300 mM NaCl, titrated to pH 8) as described in the Material and Methods. The color indicates the spectrum of ND_P at different temperatures: blue and red were obtained at 15 °C and green and purple were obtained at 50 °C. Red and purple belong to the second temperature dependent experiment.

The intensity of the resonances of POPC lipids at 15 °C and 50 °C a present similar intensity (see Figure 3.31). When ND_P sample was heated to 50 °C the peak shifted to higher frequencies and the intensity remained almost constant. Cooling the sample led to a change in the chemical shift to previous frequencies before heating and to the decrease of the resonance's intensity. When the sample was reheated the resonance shift was similar to the first temperature cycle. However, the integral of the POPC's peak after cooling decreases, due to the precipitation of lipids. As the chemical shift of ND_P returns to previous values, the electromagnetic environment of the phosphates in the NDs is similar to the initial one (i.e. before heating).

The *E. coli* lipids are a mixture of lipids, composed of three families of lipids, which are the PE, PG and CA. This heterogeneous composition of the ND_E leads to a more complex ^{31}P NMR spectrum with more peaks than those observed in the spectrum of ND_P. Initially, ^{31}P NMR spectrum of ND_E was acquired to assign the different observed peaks of the lipids' phosphate groups.

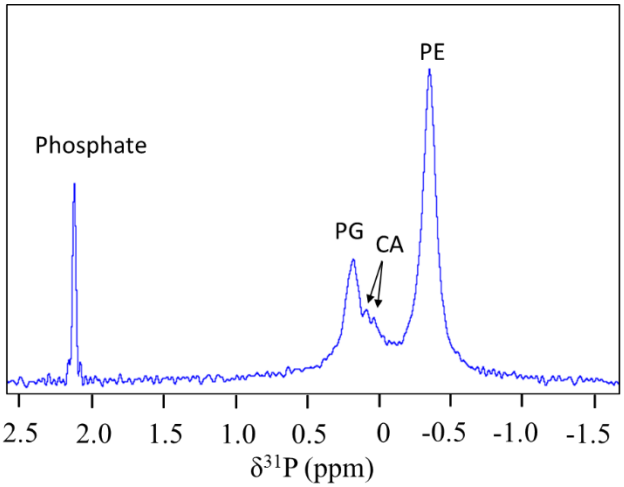

Figure 3.32: ^{31}P NMR spectrum of ND_E obtained at 15 °C (1 mM NaH_2PO_4, 40 mM Tris-HCl, 300 mM NaCl pH 8) as described in Material and Methods. The estimated concentration of ND_E is 61 µM by absorbance at 280 nm.

The ^{31} P NMR spectrum of ND_E (see Figure 3.32) shows two clear peaks and one shoulder. The peak from the phosphate buffer, which was used as a reference, is located near 2 ppm. The remaining four peaks correspond to the phosphate groups from the lipids. These peaks were assigned based on the ratio between the lipids in the sample, provided by the lipid supplier (Avanti Inc. USA, see Table 1-5), and on a rough integration of the resonances. The integration of the peaks was difficult to achieve because they were not well resolved. The areas selected for the integration were: i) the peak at lower frequencies was integrated from -0.7 ppm to -0.1 ppm, and ii) the other peaks were integrated together from -0.1 ppm to 0.5 ppm. The ratio between the two integrals, i) and ii), was close to 0.5, indicating that the concentration of the lipid, responsible for the resonance close to -0.4 ppm, is double in relation to the other lipids. With this, the resonances were assigned as follow: the peak at -0.4 ppm corresponds to the PE, the resonance near 0.2 ppm corresponds to PG and the two less intense resonances near 0 ppm correspond to the CA (CA lipid has two phosphate groups).

The ND_E were measured at different temperatures to study the behavior of the lipidic phosphate groups with the increase in temperature (see Figure 3.33a)).

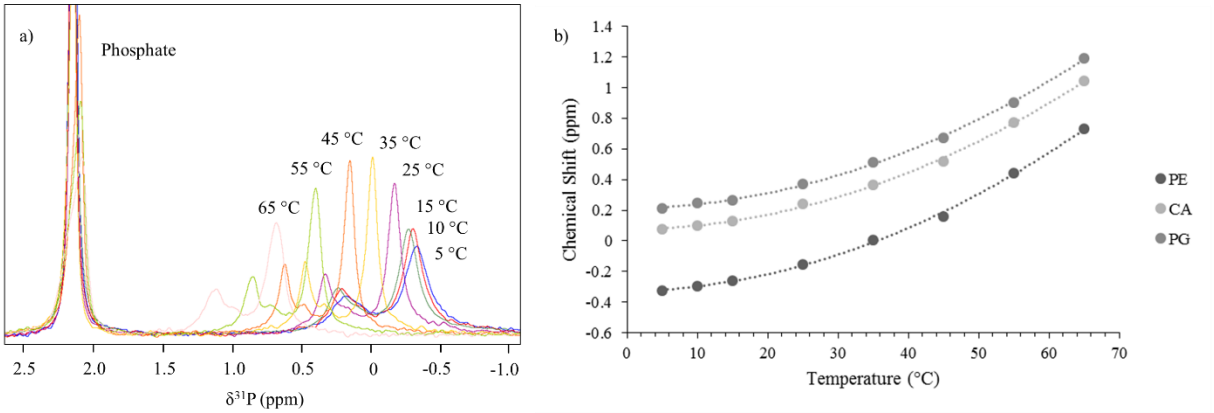

Figure 3.33: a) ^{31}P NMR spectra of ND_E obtained at different temperatures (10 mM NaH_2PO_4, 40 mM Tris-HCl, 300 mM NaCl, pH 8) as described in Material and Methods. The estimated concentration is 215 µM measured by absorbance at 280 nm. b) Plot of chemical shift as function of temperature for ND_E. Dots represent the measured values and dashed lines correspond to visual guidelines.

The ^{31}P NMR temperature dependent experiments (see Figure 3.33a)) show the chemical shift of lipids phosphate groups shifts to higher frequencies with increasing temperature. The intensity of the phosphate group peak increases until 35 °C and followed by a decrease until 65 °C. The variation of the chemical shift was plotted as function of temperature (see Figure 3.33b)). The change in the chemical shift of the peaks indicates that the electromagnetic environment of the phosphate groups changed. The change in the chemical shift can be related with the increase in diameter of the NDs, as saw by DLS measurements. The integration of the resonances was not performed because the phosphate peaks were not well resolved.

Besides the chemical shift variation, the lipids shifted differently with the increase of temperature. In order to better visualize this effect, all spectra were aligned using the resonances of the PE lipid.

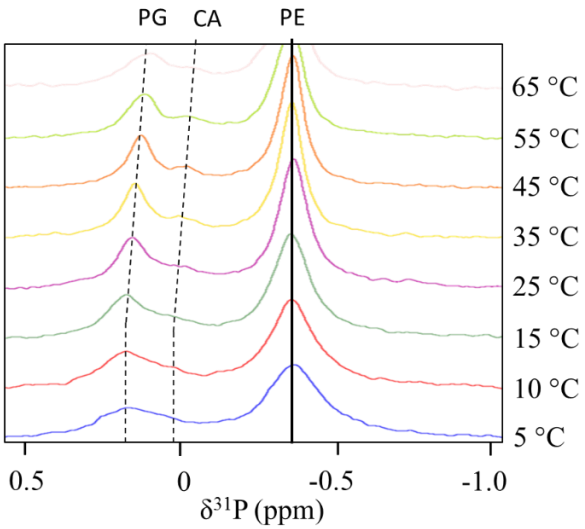

Figure 3.34: ^{31}P NMR spectra of ND_E obtained at different temperatures as described (10 mM NaH_2PO_4, 40 mM Tris-HCl, 300 mM NaCl, pH 8) in Material and Methods. The estimated concentration of ND_E is 215 µM measured by absorbance at 280 nm. Visual guidelines (dashed and full line) are shown to help the visualization of the chemical shift variation between the different lipids' phosphate peaks.

The new alignment of the phosphorus NMR spectra of ND_E (see Figure 3.35) shows that the distance between PG and PE and CA and PE peaks decrease with the increase of temperature.

This indicates that the increase of temperature affects more the PE lipid that the other two lipids. This may be explained by a different reorganization of the different lipids inside the NDs, accordingly to the respective chemical proprieties (e.g. the PE lipid can prefer an environment different of PG and CA).

In order to assess the stability of the NDs to temperature, the NMR spectra of the ND sample was measured in a temperature cycle: initially at 15 °C, heated to 65 °C afterwards it was cooled to 15 °C (as described in Figure 3.36).

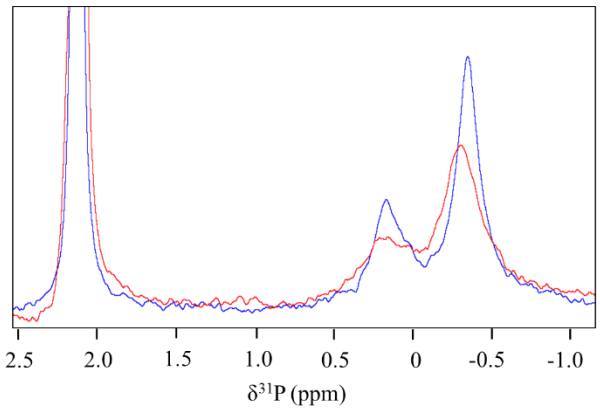

Figure 3.35: ^{31}P NMR spectra of ND_E obtained at 15 °C (10 mM NaH_2PO_4, 40 mM Tris-HCl, 300 mM NaCl, pH 8) as described in Material and Methods. The estimated concentration is 215 µM measured by absorbance at 280 nm. The blue spectrum corresponds to ND_E before the temperature dependent experiment and the red spectrum corresponds to ND_E after exposure to 65 °C.

The stability test for ND_E (see Figure 3.35) shows that the chemical shift of the peaks from the three lipids remains constant after the heating to 65 °C. This indicates the electromagnetic environment of the phosphate groups is similar before and after exposing the ND_E sample at 65 °C. On the other hand, the intensity and the integral of the resonances decreases after the exposure to 65 °C, indicating there are less lipids in solution. This effect is in agreement with the observation of precipitates after the measurements at 40 °C. These two observations confirms that the precipitates are lipids. An explanation for the precipitation of the lipids is a process called desorption. A study[80] observed this process in NDs composed with DMPC lipids from NDs by Real Time Small Angle Neutron Scattering. This happens because the lipids are highly packed in the NDs and the process of desorption is entropically favorable, but enthalpycally unfavorable. This means it is possible that small amounts of lipids in the NDs can desorb out, precipitate and destabilize the NDs. The same process of desorption can occur for the two types of characterized NDs.

The ^{31}P NMR temperature experiments did not reveal any evidence of a phase transition of the lipids, indicating that the lipids in ND_E do not undergo this process at the studied temperatures. The expected transition temperatures for this mixture of lipids are unknown, because the precise composition of the lipid mixture is unknown.

4 Conclusions

NuoL is a subunit of NADH: ubiquinone oxidoreductase involved in the transport of ions across the membrane. In this work, expression tests for the NuoL construct were performed (i.e. growth culture 6 h and 10 h after induction) and the fluorescence spectroscopy showed the tested times were not enough to express the protein. Using fluorescence spectroscopy it was shown that the expression of NuoL fused with GFP and a His tags was successful, due to a presence of a band with a maximum at 515 nm in the emission spectrum (i.e. characteristic of GFP). The purification involved two chromatography steps (IMAC and HTP), however, the final protein yield and purity was insufficient to proceed with studies. Despite the optimization of different steps in the expression and purification procedures, further studies need to be performed to obtain a higher yield of the NuoL protein. This can be achieved by testing protein expression under different conditions such as: cell growing temperature (before and after induction), cell growth duration (before after induction), concentration of the protein expression inducer (IPTG) and the aeration of the cell culture.

In this work, we also performed a biophysical characterization of the Nanodisc membrane mimicking system.

The protocol now implemented in the laboratory allows the production of different types of Nanodiscs with the specific characteristics (containing POPC or *E. coli* lipids) that will allow the reconstitution of NuoL subunit (See table 4-1).

Table 4-1: Physical characteristics of POPC and *E. coli* lipid Nanodiscs determined by size exclusion chromatography.

Experiments	**POPC (ND_P)**	***E. coli* lipids (ND_E)**
Stokes' radius (nm)	4.83	4.50; 5.20
Molecular mass (kDa)	175	139.1; 225.1

The biophysical proprieties of the Nanodiscs were investigated over a range of wide temperatures using several techniques, such as: CD, DLS, fluorescence, UV-visible and NMR spectroscopies. The results of the biophysical characterization are summarized in Table 4-2.

Table 4-2: Compilation of the results obtained by different techniques used in the biophysical characterization of POPC and *E. coli* lipid Nanodiscs. (NA – data not available)

	POPC (ND_P)		***E. coli* lipids (ND_E)**	
Experiments	Temperature dependent experiments	Stability test	Temperature dependent experiments	Stability test
DLS (nm)	10.1 ± 0.7 → 15.87 ± 0.4	NA	10.8 ± 0.3 → 16.4 ± 0.1	NA
UV-Visible spectroscopy	Absorbance remains constant at 280 nm	NA	Absorbance remains constant at 280 nm	NA
Fluorescence spectroscopy	Fluorescence intensity of tryptophans decreases with temperature	Recover of tryptophans' fluorescence intensity	Fluorescence intensity of tryptophans decreases with temperature	Recover of tryptophans' fluorescence intensity
Circular Dichroism	Loss of α-helix content with temperature	Partial recovery of α-helix content	Loss of α-helix content with temperature	Partial recovery of α-helix content
Nuclear Magnetic Resonance (^{31}P)	Peaks shift to higher frequencies	Peaks recover to initial frequency	Peaks shift to higher frequencies	Peaks recover to initial frequency

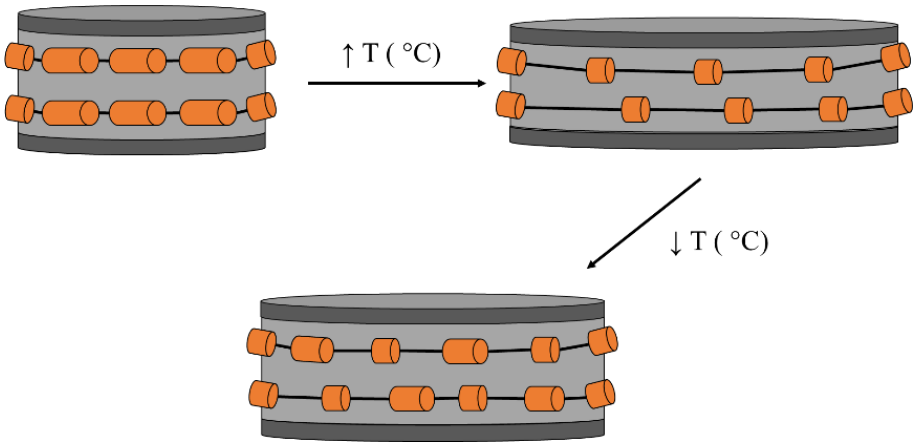

Figure 4.1: Schematic representation of Nanodiscs' behavior with changes of temperature (lipids as grey discs, MSP proteins in orange).

Combining results from the biophysical characterization (see Table 4-2), a model for describing the behavior of the Nanodiscs at different temperature was proposed (see Figure 4.1). With the increase in temperature, the Nanodiscs increase in diameter. At the same time there is a partial loss of the MSP1E1 α-helical structure (schematized in orange in Figure 4.1), allowing the Nanodiscs to expand in diameter. In parallel, the electromagnetic environment of the phosphorus present in the phospholipids changes with the increase of temperature, indicating a change in the Nanodiscs. Interestingly, after cooling, the MSP1E1s partially recover their α-helical content, suggesting the Nanodiscs could decrease in diameter

to its initial state. This observation is confirmed by ^{31}P NMR, which shows that the electromagnetic environment recovers to its initial state.

The biophysical characterization shows that the Nanodiscs are very stable at different temperatures ranges allowing studies of reconstituted proteins in different conditions (i.e. of proteins at room temperature organisms to thermophile organisms). The methodology presented here can now be used to test Nanodiscs in other conditions that will be fundamental for the study of transmembrane proteins that can be incorporated in the Nanodiscs (e.g. ionic strength and pH)

5 References

1. Nicholls, D. G. & Ferguson, J. S. *Bioenergetics 4*. (Elsevier Ltd, 2013).

2. Mitchell, P. Chemiosmotic coupling in oxidative and photosynthetic phosphorylation. *Biochim. Biophys. Acta - Bioenerg.* **1807,** 1507–1538 (2011).

3. Efremov, R. G. & Sazanov, L. a. Structure of the membrane domain of respiratory complex I. *Nature* **476,** 414–20 (2011).

4. Baradaran, R., Berrisford, J. M., Minhas, G. S. & Sazanov, L. a. Crystal structure of the entire respiratory complex I. *Nature* **494,** 443–8 (2013).

5. Efremov, R. G., Baradaran, R. & Sazanov, L. a. The architecture of respiratory complex I. *Nature* **465,** 441–5 (2010).

6. Efremov, R. G., Baradaran, R. & Sazanov, L. a. The architecture of respiratory complex I. *Nature* **465,** 441–5 (2010).

7. Efremov, R. G. & Sazanov, L. a. The coupling mechanism of respiratory complex I - a structural and evolutionary perspective. *Biochim. Biophys. Acta* **1817,** 1785–95 (2012).

8. Baradaran, R., Berrisford, J. M., Minhas, G. S. & Sazanov, L. a. Crystal structure of the entire respiratory complex I. *Nature* **494,** 443–8 (2013).

9. Sazanov, L. a. REVIEWS A giant molecular proton pump : structure and mechanism of respiratory complex I. *Nat. Publ. Gr.* **16,** 375–388 (2015).

10. Hirst, J. Mitochondrial complex I. *Annu. Rev. Biochem.* **82,** 551–75 (2013).

11. Zickermann, V. *et al.* Mechanistic insight from the crystal structure of mitochondrial complex I. **5,** 4–10

12. Vinothkumar, K. R., Zhu, J. & Hirst, J. Architecture of mammalian respiratory complex I. *Nature* (2014). doi:10.1038/nature13686

13. Batista, A. P. & Pereira, M. M. Sodium influence on energy transduction by complexes I from Escherichia coli and Paracoccus denitrificans. *Biochim. Biophys. Acta - Bioenerg.* **1807,** 286–292 (2011).

14. Søballe, B. & Poole, R. K. Microbial ubiquinones: Multiple roles in respiration, gene regulation and oxidative stress management. *Microbiology* **145,** 1817–1830 (1999).

15. Steuber, J. Na+ translocation by bacterial NADH:quinone oxidoreductases: An extension to the complex-I family of primary redox pumps. *Biochim. Biophys. Acta - Bioenerg.* **1505,** 45–56 (2001).

16. Friedrich, T., Stolpe, S., Schneider, D., Barquera, B. & Hellwig, P. Ion translocation by the Escherichia coli NADH:ubiquinone oxidoreductase (complex I). *Biochem. Soc. Trans.* **33,** 836–839 (2005).

17. Belevich, N., Belevich, G. & Verkhovskaya, M. Real-time optical studies of respiratory Complex I turnover. *Biochim. Biophys. Acta - Bioenerg.* **1837,** 1973–1980 (2014).

18. Bogachev, a V, Murtazina, R. a & Skulachev, V. P. H + /e - stoichiometry for NADH dehydrogenase I and dimethyl sulfoxide reductase in anaerobically grown Escherichia coli cells. *J. Bacteriol.* **178,** 6233–6237 (1996).

19. Wikstrom, M. & Hummer, G. Stoichiometry of proton translocation by respiratory complex I and its mechanistic implications. *Proc. Natl. Acad. Sci.* **109,** 4431–4436 (2012).

20. Treberg, J. R. & Brand, M. D. A model of the proton translocation mechanism of complex I. *J. Biol. Chem.* **286,** 17579–17584 (2011).

21. Ohnishi, T. Iron – sulfur clusters r semiquinones in Complex I. 186–206 (1998).

22. Marreiros, B. C., Batista, A. P. & Pereira, M. M. Respiratory complex I from Escherichia coli does not transport Na+ in the absence of its NuoL subunit. *FEBS Lett.* **588,** 4520–4525 (2014).

23. Moparthi, V. K., Kumar, B., Mathiesen, C. & Hägerhäll, C. Homologous protein subunits from Escherichia coli NADH:quinone oxidoreductase can functionally replace MrpA and MrpD in Bacillus subtilis. *Biochim. Biophys. Acta - Bioenerg.* **1807,** 427–436 (2011).

24. Efremov, R. G. & Sazanov, L. a. Structure of the membrane domain of Respiratory Complex 1 - Supplementary information. *Nature* **476,** (2011).

25. Kennedy, S. J. *Structures of membrane proteins. J. Membr. Biol.* **42,** (1978).

26. Michel, J., DeLeon-Rangel, J., Zhu, S., van Ree, K. & Vik, S. B. Mutagenesis of the L, M, and N subunits of complex I from escherichia coli indicates a common role in function. *PLoS One* **6,** (2011).

27. Nakamaru-Ogiso, E. *et al.* The membrane subunit NuoL(ND5) is involved in the indirect proton pumping mechanism of Escherichia coli complex I. *J. Biol. Chem.* **285,** 39070–8 (2010).

28. Torres-Bacete, J., Nakamaru-Ogiso, E., Matsuno-Yagi, A. & Yagi, T. Characterization of the NuoM (ND4) subunit in Escherichia coli NDH-1: Conserved charged residues essential for energy-coupled activities. *J. Biol. Chem.* **282,** 36914–36922 (2007).

29. Schapira, A. H. V. Mitochondrial disease. 70–82 (2006).

30. Leman, G. *et al.* Assembly defects induce oxidative stress in inherited mitochondrial complex I deficiency. *Int. J. Biochem. Cell Biol.* **65,** 91–103 (2015).

31. Raha, S. & Robinson, B. H. Mitochondria, oxygen free radicals, disease and ageing. *Trends Biochem. Sci.* **25,** 502–508 (2000).

32. Nouws, J., Nijtmans, L. G. J., Smeitink, J. a. & Vogel, R. O. Assembly factors as a new class of disease genes for mitochondrial complex i deficiency: Cause, pathology and treatment options. *Brain* **135,** 12–22 (2012).

33. Fang, H. *et al.* Exercise intolerance and developmental delay associated with a novel mitochondrial ND5 mutation. *Sci. Rep.* **5,** 10480 (2015).

34. Frick, K., Schulte, M. & Friedrich, T. Reactive Oxygen Species Production by *Escherichia coli* Respiratory Complex I. *Biochemistry* **54,** 2799–2801 (2015).

35. Lau, F. W. & Bowie, J. U. A method for assessing the stability of a membrane protein. *Biochemistry* **36,** 5884–5892 (1997).

36. T. VANAKEN, S. FOXALL-VANAKEN, S. CASTLEMAN, and S. F.-M. Alkyl Glycoside Detergents: Synthesis and Applications to the Study of Membrane Proteins. *Methods* **125,** 27–35 (1986).

37. Sanders, C. R. & Landis, G. C. Reconstitution of Membrane-Proteins Into Lipid-Rich Bilayered Mixed Micelles for Nmr-Studies. *Biochemistry* **34,** 4030–4040 (1995).

38. Czerski, L. & Sanders, C. R. Functionality of a membrane protein in bicelles. *Anal. Biochem.* **284,** 327–333 (2000).

39. Hinkle, P. C. & Cross, R. Reconstitution and Purification of the D-Glucose Transporter from Human Erythrocytes *. 7384–7391 (1977).

40. Melo, E. P., Aires-Barros, M. R. & Cabral, J. M. S. Reverse micelles and protein biotechnology. *Biotechnol. Annu. Rev.* **7,** 87–129 (2001).

41. Dmitriev, O. Y., Altendorf, K. & Fillingame, R. H. Subunit a of the E. coli ATP synthase: Reconstitution and high resolution NMR with protein purified in a mixed polarity solvent. *FEBS Lett.* **556,** 35–38 (2004).

42. Tribet, C., Audebert, R. & Popot, J. L. Amphipols: polymers that keep membrane proteins soluble in aqueous solutions. *Proc. Natl. Acad. Sci. U. S. A.* **93,** 15047–15050 (1996).

43. Bayburt, T. H., Grinkova, Y. V. & Sligar, S. G. Self-Assembly of Discoidal Phospholipid Bilayer Nanoparticles with Membrane Scaffold Proteins. *Nano Lett.* **2,** 853–856 (2002).

44. Denisov, I. G., Grinkova, Y. V, Lazarides, a a & Sligar, S. G. Directed self-assembly of monodisperse phospholipid bilayer Nanodiscs with controlled size. *J. Am. Chem. Soc.* **126,** 3477–87 (2004).

45. Shih, A. Y., Arkhipov, A., Freddolino, P. L., Sligar, S. G. & Schulten, K. Assembly of lipids and proteins into lipoprotein particles. *J. Phys. Chem. B* **111,** 11095–104 (2007).

46. Warschawski, D. E. *et al.* Choosing membrane mimetics for NMR structural studies of transmembrane proteins. *Biochim. Biophys. Acta - Biomembr.* **1808,** 1957–1974 (2011).

47. Seddon, A. M., Curnow, P. & Booth, P. J. Membrane proteins, lipids and detergents: Not just a soap opera. *Biochim. Biophys. Acta - Biomembr.* **1666,** 105–117 (2004).

48. Shen, H. H., Lithgow, T. & Martin, L. L. Reconstitution of membrane proteins into model membranes: Seeking better ways to retain protein activities. *Int. J. Mol. Sci.* **14,** 1589–1607 (2013).

49. Henry, G. D. & Sykes, B. D. Methods to study membrane protein structure in solution. *Methods Enzymol.* **239,** 515–535 (1994).

50. Ritchie, T. K. *et al. Chapter 11 - Reconstitution of membrane proteins in phospholipid bilayer nanodiscs. Methods Enzymol.* **464,** (Elsevier Inc., 2009).

51. Glu, J. M., Wittlich, M., Feuerstein, S., Hoffmann, S. & Willbold, D. Integral Membrane Proteins in Nanodiscs Can Be Studied by Solution NMR Spectroscopy spectroscopy is limited by slow rotational diffusion of the particles . *J. Am. Chem. Soc.* **131,** 12060–12061 (2009).

52. Hagn, F., Etzkorn, M., Raschle, T. & Wagner, G. Optimized phospholipid bilayer nanodiscs facilitate high-resolution structure determination of membrane proteins. *J. Am. Chem. Soc.* **135,** 1919–1925 (2013).

53. Bayburt, T. H. & Sligar, S. G. Membrane protein assembly into Nanodiscs. *FEBS Lett.* **584,** 1721–7 (2010).

54. Wadsäter, M., Barker, R., Mortensen, K., Feidenhans'L, R. & Cárdenas, M. Effect of phospholipid composition and phase on nanodisc films at the solid-liquid interface as studied by neutron reflectivity. *Langmuir* **29,** 2871–2880 (2013).

55. Bayburt, T. H., Grinkova, Y. V. & Sligar, S. G. Assembly of single bacteriorhodopsin trimers in bilayer nanodiscs. *Arch. Biochem. Biophys.* **450,** 215–222 (2006).

56. Denisov, I. G., McLean, M. a., Shaw, A. W., Grinkova, Y. V. & Sligar, S. G. Thermotropic phase transition in soluble nanoscale lipid bilayers. *J. Phys. Chem. B* **109,** 15580–15588 (2005).

57. Wadsäter, M., Maric, S., Simonsen, J. B., Mortensen, K. & Cardenas, M. The effect of using binary mixtures of zwitterionic and charged lipids on nanodisc formation and stability. *Soft Matter* **9,** 2329 (2013).

58. Sušac, L., Horst, R. & Wüthrich, K. Solution-NMR characterization of outer-membrane protein A from E. coli in lipid bilayer nanodiscs and detergent micelles. *Chembiochem* **15,** 995–1000 (2014).

59. Dalal, K., Chan, C. S., Sligar, S. G. & Duong, F. Two copies of the SecY channel and acidic lipids are necessary to activate the SecA translocation ATPase. *Proc. Natl. Acad. Sci.* (2012). doi:10.1073/pnas.1117783109

60. Denisov, I. G. & Sligar, S. G. Cytochromes P450 in nanodiscs. *Biochim. Biophys. Acta* **1814,** 223–9 (2011).

61. J.H. Morrissey, V. Pureza, R.L. Davis-Harrison, S.G. Sligar, C.M. Rienstra, A.Z. Kijac, Y. Z. Ohkubo, and E. T. Protein-membrane interactions: Blood clotting on nanoscale bilayers. *J Thromb Haemost* **29,** 997–1003 (2012).

62. Leitz, A. J., Bayburt, T. H., Barnakov, A. N., Springer, B. a. & Sligar, S. G. Functional reconstitution of ??2-adrenergic receptors utilizing self-assembling Nanodisc technology. *Biotechniques* **40,** 601–612 (2006).

63. Boldog, T., Grimme, S., Li, M., Sligar, S. G. & Hazelbauer, G. L. Nanodiscs separate chemoreceptor oligomeric states and reveal their signaling properties. *Proc. Natl. Acad. Sci. U. S. A.* **103,** 11509–11514 (2006).

64. Alami, M., Dalal, K., Lelj-Garolla, B., Sligar, S. G. & Duong, F. Nanodiscs unravel the interaction between the SecYEG channel and its cytosolic partner SecA. *EMBO J.* **26,** 1995–2004 (2007).

65. Numata, M. *et al.* Nanodiscs as a therapeutic delivery agent: Inhibition of respiratory syncytial virus infection in the lung. *Int. J. Nanomedicine* **8,** 1417–1427 (2013).

66. Das, A., Zhao, J., Schatz, G. C., Sligar, S. G. & Van Duyne, R. P. Screening of type I and II drug binding to human cytochrome P450-3A4 in nanodiscs by localized surface plasmon resonance spectroscopy. *Anal. Chem.* **81,** 3754–3759 (2009).

67. Carney, C. E. *et al.* Nanodiscs as a Modular Platform for Multimodal MR-Optical Imaging. *Bioconjug. Chem.* 150409155603005 (2015). doi:10.1021/acs.bioconjchem.5b00107

68. Ham, M.-H. *et al.* Photoelectrochemical complexes for solar energy conversion that chemically and autonomously regenerate. *Nat. Chem.* **2,** 929–936 (2010).

69. Kobayashi, Y. & Kawamura, F. *Molecular cloning. Biotechnology* **22,** (1992).

70. Frigon, R. P., Leypoldt, J. K., Uyeji, S. & Henderson, L. W. Disparity between Stokes radii of dextrans and proteins as determined by retention volume in gel permeation chromatography. *Anal. Chem.* **55,** 1349–54 (1983).

71. Wyss, M. *et al.* Biophysical characterization of fungal phytases (myo-inositol hexakisphosphate phosphohydrolases): Molecular size, glycosylation pattern, and engineering of proteolytic resistance. *Appl. Environ. Microbiol.* **65,** 359–366 (1999).

72. Meirelles, G. V *et al.* Human Nek6 is a monomeric mostly globular kinase with an unfolded short N-terminal domain. *BMC Struct. Biol.* **11,** 12 (2011).

73. Cavanagh, J., Fairbrother, W., Iii, A. P. & Skelton, N. *Protein NMR Spectroscopy, 2nd Edition Principles and Practice*. *Curr. Biol.* (2007).

74. Geertsma, E. R., Groeneveld, M., Slotboom, D.-J. & Poolman, B. Quality control of overexpressed membrane proteins. *Proc. Natl. Acad. Sci. U. S. A.* **105,** 5722–5727 (2008).

75. Lakowicz, J. R. *Principles of Fluorescence Spectroscopy Joseph R . Lakowicz*.

76. Guilbault, G. G. *Practical fluorescence*. *Circulation* **2nd Editio,** (1990).

77. Kelly, S. M., Jess, T. J. & Price, N. C. How to study proteins by circular dichroism. *Biochim. Biophys. Acta* **1751,** 119–39 (2005).

78. Triba, M. N., Warschawski, D. E. & Devaux, P. F. Reinvestigation by Phosphorus NMR of Lipid Distribution in Bicelles. *Biophys. J.* **88,** 1887–1901 (2005).

79. Glover, K. J. *et al.* Structural Evaluation of Phospholipid Bicelles for Solution-State Studies of Membrane-Associated Biomolecules. **81,** 2163–2171 (2001).

80. Nakano, M. *et al.* Static and Dynamic Properties of Phospholipid Bilayer Nanodiscs. 8308–8312 (2009).

6 Appendices

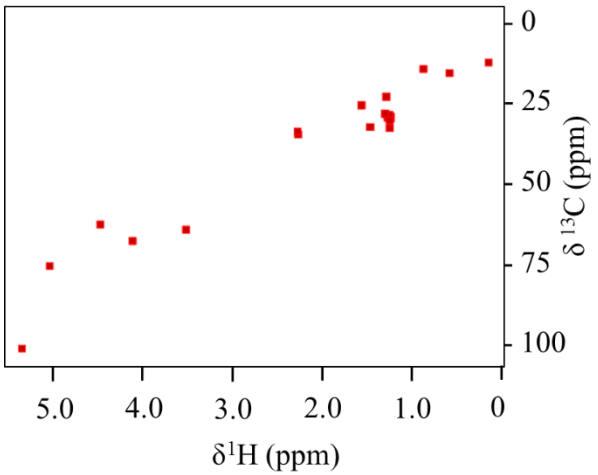

Figure 6.1: ^{1}H-^{13}C HSQC prediction spectrum of PG. (From http://www.nmrdb.org/)

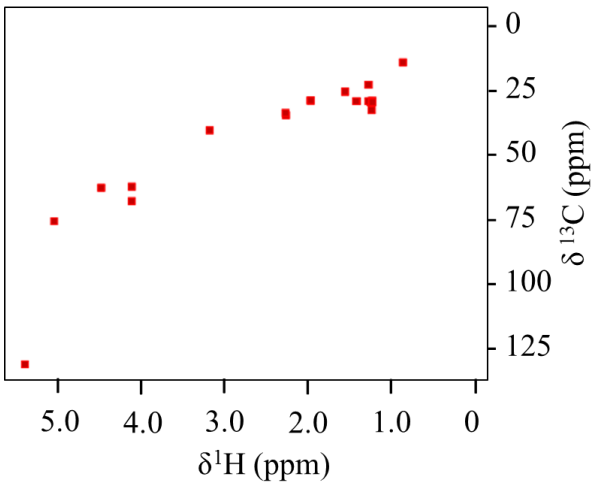

Figure 6.2: ^{1}H-^{13}C HSQC prediction spectrum of PE. (From http://www.nmrdb.org/)

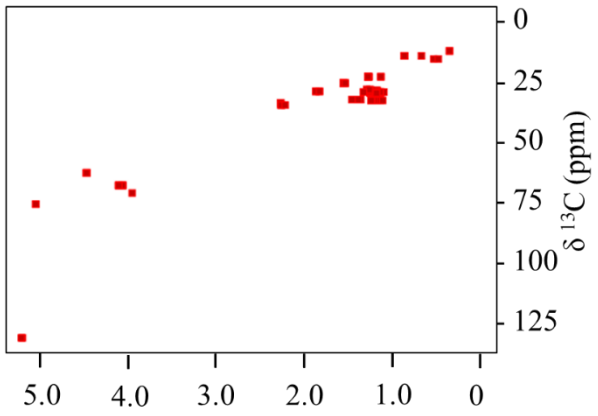

Figure 6.3: ^{1}H-^{13}C HSQC prediction spectrum of CA. (From http://www.nmrdb.org/)